EXPLORING A NOVEL ENERGY-RECOVERING ARCHITECTURE FOR HYDRAULIC ACTUATION

A Thesis
Presented to
The Academic Faculty

by

Oscar R. Peña

In Partial Fulfillment
of the Requirements for the Degree
Master of Science in the
School of Mechanical Engineering

Georgia Institute of Technology
August 2016

EXPLORING A NOVEL ENERGY-RECOVERING ARCHITECTURE FOR HYDRAULIC ACTUATION

Approved by:

Dr. Michael J. Leamy, Advisor
School of Mechanical Engineering
Georgia Institute of Technology

Dr. Aldo A. Ferri
School of Mechanical Engineering
Georgia Institute of Technology

Dr. Jun Ueda
School of Mechanical Engineering
Georgia Institute of Technology

Date Approved: May 20th, 2016

Dedicado a mi mami, mi papi, y mis ñaños

ACKNOWLEDGEMENTS

I would like to thank, above all, my advisor Dr. Michael Leamy whose time and expertise was vital to my research. From beginning to end Dr. Leamy guided me along a path of quality and challenging research culminating in this thesis and the acquisition of my Master's degree. I would also like to thank Dr. Aldo Ferri and Dr. Jun Ueda who agreed to use their time to serve on my thesis committee and provide valuable feedback. Additionally, I would like to thank Dr. Sarina Ergas, Dr. Jeffrey Cunningham, and Dr. Maureen Kinyua without whom I would have not made the decision to step into graduate school, much less into a research environment.

I also extend my gratitude to my lab mates Jason Kulpe, Justin Wilbanks, Saeid Loghavi, Matt Fronk, Amir Darabi, and Douglas Cox with whom I shared conversations and experiences, both academic and recreational, that taught me many things and helped make my graduate studies enjoyable.

Finally, I would like to thank those who will always be constants in life, my parents and brothers, whose support always makes any challenge easier by assuring me that a hand will always be there to help me up from my falls.

TABLE OF CONTENTS

LIST OF TABLES

LIST OF FIGURES

LIST OF SYMBOLS

ΔP	Pressure differential across a component
P_o	Initial pressure in an accumulator
k	Energy storage coefficient of an accumulator
q	Fluid flow
c	Fluid damping coefficient
T	Shaft torque
T_{fr}	Frictional torque
D	PM displacement
ω	Shaft speed
q_L	Leakage flow
$P_{cylinder}$	Pressure at cap side of hydraulic cylinder
P	Pressure in accumulator
m	Cab mass
A	Cross-sectional area of cap side of hydraulic cylinder
g	Gravitational acceleration
I	Integral gain of feedback controller
P	Proportional gain of feedback controller
e	Error signal associated with feedback controller
E_{cab}	Energy provided to or by elevator cab
E_2	Energy provided to or by Accumulator 2
E_1	Energy provided to or by Accumulator 1
E_{tot}	Total energy flow through the system
k_{L1}	Volumetric efficiency proportionality coefficient

ΔP_{nom}	Nominal pressure of PM
D_{max}	Maximum displacement of PM
ω_{nom}	Nominal shaft speed of PM
k_{LP}	Volumetric efficiency pressure coefficient
k_{LD}	Volumetric efficiency displacement coefficient
k_{Lm}	Volumetric efficiency angular velocity coefficient
k_{FP}	Mechanical efficiency pressure coefficient
k_{FD}	Mechanical efficiency displacement coefficient
k_{Fm}	Mechanical efficiency angular velocity coefficient
k_{F1}	Mechanical efficiency proportionality coefficient
n	Machine type coefficient
η_{mp}	Mechanical efficiency while pumping
η_{mm}	Mechanical efficiency while motoring
η_{vp}	Volumetric efficiency while pumping
η_{vm}	Volumetric efficiency while motoring
$\eta_{system1}$	Total efficiency of present system
E_{out}	Energy flow out of hydraulic PM(s)
E_{in}	Energy flow into hydraulic PM(s)
E_{EM}	Energy flow out of electric machine
$\eta_{system2}$	Total efficiency of electrohydraulic system
$E_{accumulator}$	Energy provided to or by an accumulator
$E_{battery}$	Energy provided to or by a battery
P_{losses}	Power losses in electric machine
k_c	Electrical resistance efficiency coefficient
k_i	Magnetic loss efficiency coefficient

k_ω	Friction and windage efficiency coefficient
C	Miscellaneous loss constant
η_m	Efficiency of electric motor
P_{out}	Power output of electric machine
P_{in}	Power input of electric machine
η_g	Efficiency of electric generator
A_{req}	Minimum area allowed for hydraulic cylinder
m_{max}	Maximum mass on hydraulic cylinder
a_{max}	Maximum acceleration of hydraulic cylinder
P_{cmax}	Maximum allowed pressure on hydraulic cylinder
V_{fluid}	Maximum fluid volume in an accumulator
h_{max}	Maximum extension of hydraulic cylinder
P_{max}	Maximum operating pressure of an accumulator
U	Maximum stored energy in an accumulator
m_{min}	Minimum mass on hydraulic cylinder
P_{pr}	Pre-charge pressure of an accumulator
q_{max}	Maximum flow in a fluid domain
v_{max}	Maximum velocity of hydraulic cylinder
m_{person}	Mass of a single person
V	Accumulator size
Pa	Atmospheric Pressure
x_k	State variable in Dynamic Programming
u_k	Control variable in Dynamic Programing
F_k	State transition in Dynamic Programming
$J_{0,\pi}$	Total cost in Dynamic Programming

$g_{0/N}$	Initial/Final constraints in Dynamic Programming
ϕ_k	Penalty costs in Dynamic Programming
h_k	Incremental cost in Dynamic Programming
T_{EM}	Electric motor torque
Δt	Incremental Time in Dynamic Programming

SUMMARY

This thesis begins through the introduction of a novel hydraulic actuation architecture and proceeds with the development of said architecture with respect to its control, sizing, and efficiency. Hydraulic actuation is used in several important industries today. It is commonly sought after due to its high power density. Like in most power transfer technologies, hydraulic actuation is often the target of efforts at improving its efficiency. Chapter 2 of this thesis introduces a novel hydraulic actuation architecture that shows promising efficiency advantages over contemporary architectures. Specifically, the introduced architecture achieves controlled actuation without relying on the use of throttling; an ubiquitous practice used to achieve controlled motion within fluid power which dissipates large amount of energy. The merits of the introduced architecture are identified, in the context of the hydraulic elevator, against a traditional throttle-based architecture and further validated against a state-of-the-art electrohydraulic architecture.

The varying effect of sizing and control on the resulting efficiency necessitated the development of strategies which allow for an informed determination of both. To this end, Chapter 3 of this thesis employs Dynamic Programming (DP) in a backward-looking simulation of the system to inform both sizing and control of the architecture and move beyond the heuristic approach used in Chapter 2. DP-Informed Monte Carlo simulations allow for an optimal sizing region to be determined. Subsequently, DP-Informed rule-based control of the system is developed and implemented in a forward-looking simulation. The resulting system is compared to initial heuristic attempts at sizing and control and shown to have a considerable improvement. Finally, the architecture is further explored in the context of a hydraulic forklift. Dynamic Programming and Monte Carlo simulations are again employed to develop forward-looking simulation of the architecture. The resulting system is determined to be moderately optimal. Suggested

future work involves the creation of a prototype and attempts at commercialization. It is expected that the introduced hydraulic architecture is applicable in many industries.

CHAPTER 1

INTRODUCTION AND BACKGROUND

1.1 Motivation

The practice of converting hydrostatic fluid power into translational or rotational mechanical power is ubiquitous in many industries today. Typically, the power transfer happens through a hydraulic actuator in hydraulic communication with an appropriate hydraulic circuit, and in mechanical communication with its surroundings, such that desired motion is achieved. Common in most forms of power transfer, hydraulic actuation often also has as its goal the movement of a load through a desired motion profile. Achieving movement of a certain load simply requires enough energy to be input. However, controlled motion of the load requires more nuanced techniques which vary in efficacy and efficiency.

In general, two approaches achieve motion control of a hydraulic actuator, fluid throttling and displacement control. Motion control via fluid throttling (typically implemented with a load sensing circuit) controls flow into the actuator. Throttling (via flow-control valves) is easily and inexpensively implemented and has a high bandwidth due to the small inertia associated with the throttle valve moving parts. On the other hand, throttling acts by dissipating energy as heat, which renders it highly inefficient [1-3]. In contrast, a desired motion profile can also be achieved by controlling the flow output of the pump (displacement control), either via a variable-speed electric motor actuating a fixed-displacement pump, or a variable-displacement pump controlled by a single speed electric drive. Displacement control can entirely eliminate the need for throttling, and therefore the dissipation of energy associated with it, but has a low bandwidth [4-7].

Additionally, in multiple actuation systems (such as an excavator), a pump for each actuator is needed, resulting in upfront costs much higher than a valve-controlled multi-actuator system; although improvement in overall efficiency can offset costs in the long run [7]. Many industries today require controlled motion of hydraulic actuation; nonetheless, a large part of them still employ throttling control to meets those requirements. Improving motion control techniques would have a large impact in many industries today and energy usage worldwide.

1.2 Hydraulic Elevator Review

The hydraulic elevator in particular has suffered from high inefficiency stemming from a heavy reliance on throttling-based control. In general, upon descent, the hydraulic elevator will be controlled through the use of servo valve which dissipates much of its potential energy. This inefficiency largely accounts for its lost market share to traction elevators. In 1986 sales of hydraulic elevators were over 60% higher than those of traction elevators worldwide [8]. By 1995, this figure began decreasing due to the introduction of machine room-less (MRL) traction elevators, and has recently reached a market share as low as 40% worldwide while approximately two thirds of new elevators are MRLs since 2010 [9]. Additionally, traction elevators boast the benefit of an easily implemented counterweight, further improving their efficiency. Even on mechanically counterweighted hydraulic elevators, the use of throttling valves while descending and stopping dissipates significant energy and negatively impacts the hydraulic elevator's efficiency. Nevertheless, fluid power has advantages over mechanical power transfer, such as high power density, that warrant efforts aimed at improving hydraulic elevator efficiency, especially in low-speed, high pressure applications [10, 11].

1.2.1 Contemporary Hydraulic Elevator Architectures

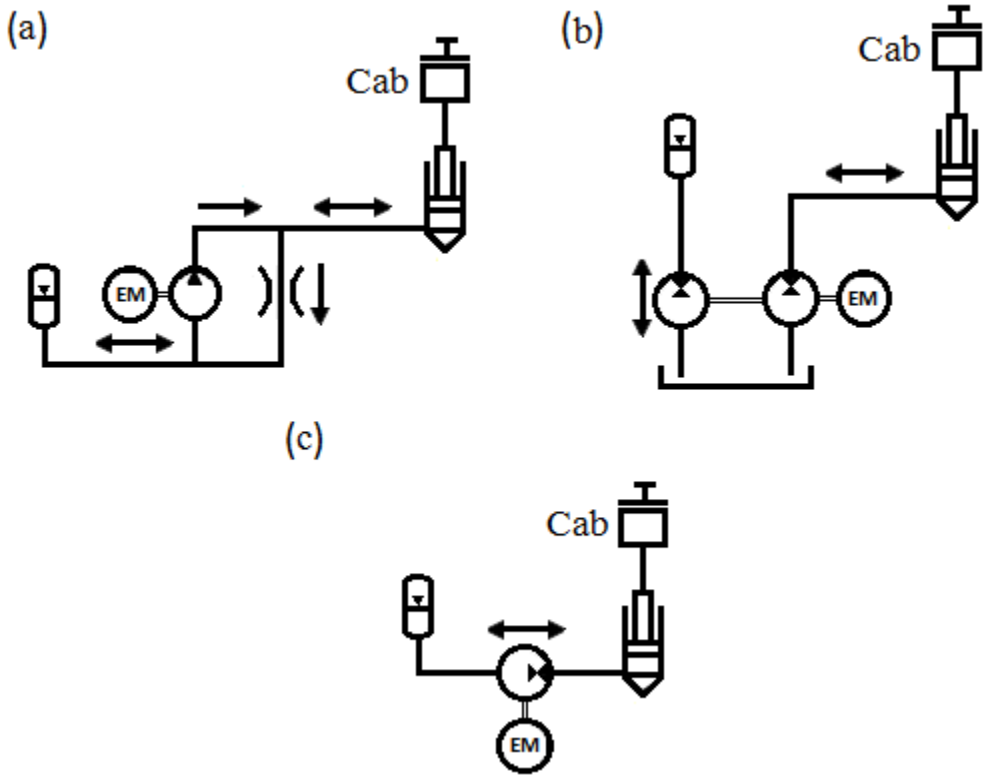

Figure 1.1: Examples of relevant hydraulic elevator architectures in the literature: (a) valve-controlled, hydraulically counterweighted elevator, (b) elevator hydraulically counterweighted via a hydraulic transformer, (c) hydraulically counterweighted elevator with regenerative braking via an electric generator.

Investigation into the improvement of hydraulic elevators remains active and ongoing since their inception in 1878 by Otis Brothers Co. [12], although research on improving efficiency has been a more recent endeavor. In his attempt at an early efficiency improvement, Edwards introduced the concept of a hydraulic counterweight by suggesting the use of a pressurized oil source to capture energy from the cab on its way down [13]. Ran studied such a system by incorporating an accumulator as the main oil source in a valve-controlled hydraulic elevator, as shown in Figure 1.1(a) [14]. In these

systems, the accumulator reduces the pressure differential across the pump, thereby reducing the energy input needed from the electric motor. Descent and ascent of the cab is still regulated via a throttling valve that diverts extra flow during upward motion and restricts flow during downward motion, as needed, to meet a motion profile. The system also has an auxiliary pump system to compensate for leakage over time.

In 1992, researchers from Mitsubishi Electric introduced the first displacement-controlled hydraulic elevator using a variable-speed motor [15]. Researchers from Bucher Hydraulics also used displacement control and a hydraulic counterweight in communication with the cab via a hydraulic transformer to significantly reduce throttling (Figure 1.1(b)). Xu further expanded on the concept with several investigations on its movement and efficiency [2, 16-18]. In these architectures, the main speed control component, an electric motor, regulates the torque to the PM in hydraulic communication with the cab. The accumulator supplements the torque provided by the electric motor via its PM during upward motion and reduces the amount of braking torque required during descent. This system almost entirely eliminates the need for a throttling valve and its associated inefficiencies.

Researchers from Bucher Hydraulics further improved this idea by eliminating the hydraulic transformer and using an accumulator again as the primary oil source. Yang studied this idea in detail and provided some insights into its relative efficiency [19, 20]. In such a design (Figure 1.1(c)), the main speed control component, again an electric motor/generator, provides and absorbs torque from the system as needed. A highly efficient electrohydraulic design was achieved through the use of an electric generator to recapture some of the energy dissipated by the braking torque. The merits of the electrohydraulic design will be compared and contrasted with the hydraulic design

introduced herein. A detailed schematic of the system is reproduced from Yang's work in Figure A1.

The large potential for improvement in the hydraulic elevator positions it as good technology to explore; as such, this thesis will focus primarily on the advantages of the hydraulic design introduced herein within the context of the hydraulic elevator.

1.3 Hydraulic Forklift Review

The hydraulic forklift is another technology that suffers from high inefficiencies caused by throttling. In general, the hydraulic forklift uses an electric battery to supply a pump which in turn supplies power to an actuator upon lifting. On descent, however, the hydraulic forklift will dissipate much of its potential energy through the use of throttling, recovering little to no energy. Attempts at remedying this inefficiency have also been undertaken for the hydraulic forklift. Minav's work uses a speed-controlled motor to achieve displacement control of the forklift and bypass throttling, additionally, an attempt to recover electrical energy so as to extend the life of the battery is also performed [21, 22]. A schematic of the test setup can be seen in Figure A2 in Appendix A. The hydraulic forklift will be visited in Chapter 3 as a second technology which may benefit from the hydraulic architecture introduced herein. A less extensive study of the introduced architecture within the context of the hydraulic forklift is also performed in this thesis.

CHAPTER 2

AN EFFICIENT ARCHITECTURE FOR ENERGY RECOVERY IN HYDRAULIC ACTUATION

2.1 Introduction

Chapter 2 of this thesis introduces an efficient architecture for hydraulic actuation that offers capability for controlled motion while bypassing throttling. A physical model of the architecture is developed and posed as a single-input single-output (SISO) system in which the ratio of two hydraulic pump/motor swash plate angles serve as the control input for regulating the output actuation speed. The architecture is explored in the context of a hydraulic elevator due to the potential for improvement within the industry. Accordingly, heuristic control rules based on efficiency considerations and elevator operation are posed for the swash plate angles. A high-fidelity simulation tool is then employed to assess the new architecture and control approach. Simulations demonstrate the effectiveness of the devised control strategy and the overall satisfactory operation of the elevator system. Simulations also provide comparisons of the new architecture's efficiency versus an electrohydraulic elevator architecture employing a motor/generator for energy capture and return. It's shown that the introduced architecture yields up to a 13% increase in actuation efficiency over the electrohydraulic system, and up to a 23% reduction in input energy over a day's operation.

2.2 Novel Hydraulic Architecture

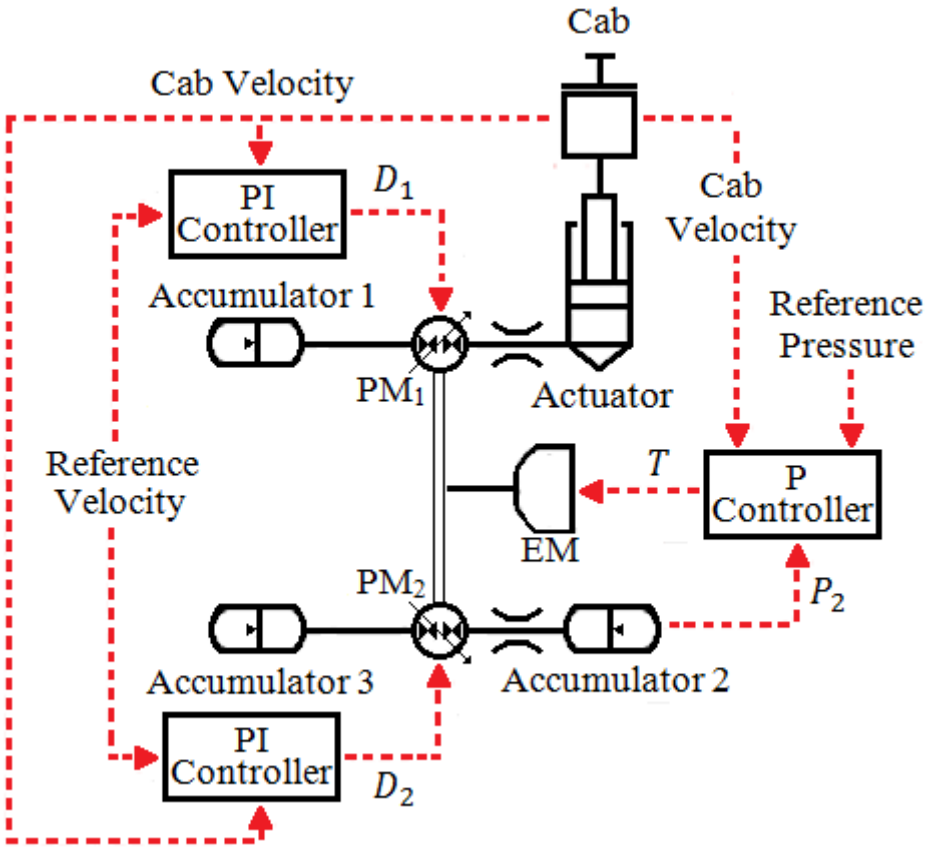

Figure 2.1: Introduced architecture and accompanying controllers.

Although not conceived as such, the hydraulic architecture introduced herein can be arrived at through a modification of the design introduced by Bucher Hydraulics, Figure 1.1(c). By eliminating the electric motor and replacing it with a hydraulic transformer connected to two accumulators, as shown in Figure 2.1, an architecture results which eliminates the mechanical to electrical energy conversion, and all the associated peripherals (connection to utilities, battery, converter, etc.) present in the Bucher Hydraulics system. The drawback of the accumulator being characterized by much lower energy density than a battery is of little consequence in stationary applications, such as the elevator [23]. There are 7 primary components in the proposed dual

pump/motor speed-controlling hydraulic architecture: two variable-displacement pump/motors, two accumulators, a small auxiliary electric motor (*not* a motor/generator), an actuator, and a reservoir or low-pressure auxiliary accumulator. The main accumulator (Accumulator 1) serves as the main source of fluid for actuation. This connects to the actuator via a main pump/motor (PM_1) that shuttles fluid between the actuator and Accumulator 1. A second pump/motor (PM_2) connects to PM_1 through a shaft and shuttles fluid from a reservoir or low pressure accumulator (Accumulator 3) to a secondary accumulator (Accumulator 2). A small electric machine (EM) serves as a supplemental power source which operates either PM_1 or PM_2 to restore lost energy in the system due to system losses such as hydraulic friction, fluid leakage in PM_1 or PM_2, etc. Control of the system can be achieved by varying the displacements in the PM_1-shaft-PM_2 assembly (the hydraulic transformer).

The use of a hydraulic transformer with variable displacement PMs for motion control of hydraulic actuation is also used by Hung *et al.* [24]. Although their motion control method contains similarities to the system introduced herein, key differences are present which render the introduced architecture novel. Principally, in the absence of losses, an external power source is eliminated and thus the system becomes driven exclusively by its pre-charged accumulators. A hydraulic pump driven by an EM acts as the main source of power input into Hung's system. Secondarily, in a typical implementation of the hydraulic transformer, the PMs share a pressure node, as shown in Hung's work. By eliminating this hydraulic communication, a versatile operation arises which includes freely designing for pressure differentials and flow through each individual PM, thus allowing for their most efficient use.

The proposed architecture can operate in two different modes, which in summary reduce to Accumulator 2 providing power to lower the load, hereafter referred to as Mode 1, or

Accumulator 2 providing power to lift the load, hereafter referred to as Mode 2. In Mode 1, cylinder extension is achieved by utilizing Accumulator 1 as the power source while energy is stored in Accumulator 2 via PM_2 working as a pump powered by PM_1 (itself acting as a motor). Cylinder contraction is achieved by utilizing Accumulator 2 as the main power source to drive PM_2 which, in turn, powers PM_1 and pumps fluid from the actuator to Accumulator 1, thereby lowering the cab and recharging Accumulator 1. In Mode 2, cylinder extension is achieved by utilizing Accumulator 2 to drive PM_2 (as a motor), which in turn drives PM_1 to pump fluid from Accumulator 1 to the actuator, thereby raising the cab. Cylinder contraction is achieved by letting the gravitational potential energy of a lifted load drive PM_1 (as a motor), which in turn drives PM_2 (as a pump) and thereby recharges Accumulator 2. Figure B1 in Appendix B introduces a visual depiction of the energy flow through the architecture in each mode. In either mode described above, the variable displacement that characterizes the PMs allows the torque to vary across the shaft as a function of the two displacements, thereby acting as an efficient and controllable speed governor.

2.2.1 Analytical Model

Hydraulic circuits are inherently nonlinear due to the nonlinear relationship between differential pressure and flow in many hydraulic components. Specifically, for this system, gas-charged accumulators and the damping effects of the fluid conduits (tubing, valves, etc.) are both nonlinear. Due to the complexities that arise from the nonlinearity when obtaining mathematical models, a representation of the system using linear components, such as the spring-loaded accumulator and linear hydraulic resistances, are used in developing the initial heuristic control scheme. A fully nonlinear simulator in Section 2.2.2 tests the efficacy of the developed controllers.

The following equations describe the relationship between differential pressure and flow in the linear accumulator, and hydraulic resistance of a conduit, respectively,

$$\Delta P = P_o + k \int q \, dt \tag{1}$$

$$\Delta P = cq \tag{2}$$

where q denotes volumetric flow, ΔP the differential pressure, P_o the precharge/initial pressure in the accumulator, c the damping coefficient, and k the energy storage coefficient of an accumulator. The damping coefficient, c, represents all sources of losses due to flow resistance, such as valves, the hydraulic cylinder, and piping.

Additionally, the relationship between the torque, T, and pressure differential across a PM is given by,

$$\Delta P = \frac{T \pm T_{fr}}{D} \tag{3}$$

where T_{fr} denotes the friction torque for which the sign depends on whether the PM is motoring (positive) or pumping (negative); D refers to the displacement of the PM, which is given by the combination of q and leakage losses, q_L, divided by the angular velocity of the shaft, ω, as given in (4). Leakage losses change sign depending on whether the PM is motoring (negative) or pumping (positive),

$$D = \frac{q \mp q_L}{\omega} \tag{4}$$

To derive state equations, this work invokes an electric circuit approach and the concept of through and across variables, q and ΔP, respectively. In complete analogy to an electric circuit, the variable q remains constant through all pressure nodes in series while a pressure differential is associated with flow across each component. By determining

the pressure nodes of the system (at each end of every hydraulic component), the relationships given by (1) - (3) between differential pressure and flow across each component, as shown in Figure 2.2, serve to derive the governing equations for both the top and the bottom hydraulic circuits.

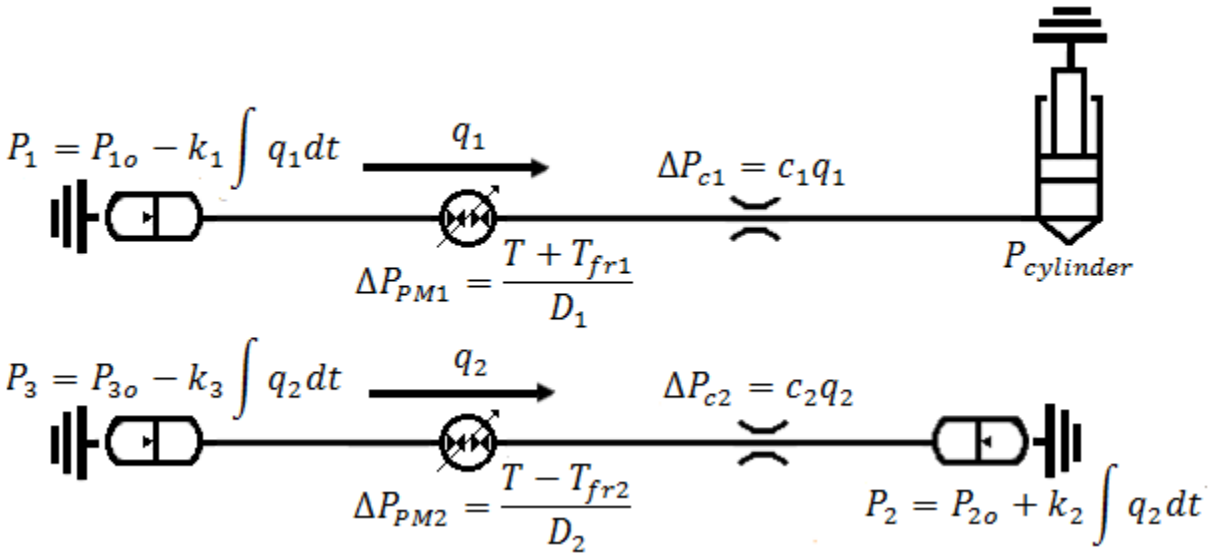

Figure 2.2: Hydraulic circuit representation of top and bottom fluid domains

Using the hydraulic equivalent of Kirchhoff's loop law, one can arrive at (5) and (6) for the top and bottom fluid domains, respectively:

$$P_1 - \Delta P_{PM1} - \Delta P_{c1} - P_{cylinder} = 0 \tag{5}$$

$$P_3 + \Delta P_{PM2} - \Delta P_{c2} - P_2 = 0 \tag{6}$$

Using Newton's 2nd law on the cab of mass m, and recognizing that $\frac{1}{A}\frac{dq_1}{dt}$ gives the acceleration of the cab, one finds an expression for $P_{cylinder}$,

$$P_{cylinder} = \frac{m}{A^2}\frac{dq_1}{dt} + \frac{mg}{A} \tag{7}$$

Furthermore, by reasonably neglecting shaft inertia torques in comparison to PM inertias, the torque experienced by both PM's is assumed equal. Using this relationship and recognizing that the flows (q_1, q_2) are related by the angular speed of the shaft and

the PM displacements ($\frac{q_2+q_{L2}}{D_2} = \frac{q_1-q_{L1}}{D_1}$), one arrives at a Single-Input Single-Output (SISO) model of the system, with pressures as indicated in Figure 2.2, where the input is the ratio of displacements $\frac{D_2}{D_1}$ and the output is the flow q_1, which directly relates to the cab velocity by the area, A:

$$\frac{m}{A^2}\frac{dq_1}{dt} + \left(c_1 + \left(\frac{D_2}{D_1}\right)^2 c_2\right) q_1 + k_1 \int q_1 dt + \frac{D_2}{D_1}(k_2 + k_3) \int \frac{D_2}{D_1} q_1 dt$$

$$= P_{1o} - \frac{mg}{A} - \frac{D_2}{D_1}(P_{2o} - P_{3o}) + \left(\frac{T_{fr_2} + T_{fr_1}}{D_1}\right) + c_2 \frac{D_2}{D_1}\left(\frac{D_2}{D_1} q_{L_1} - q_{L_2}\right) \qquad (8)$$

$$+(k_2 + k_3)\frac{D_2}{D_1} \int q_{L_2}\, dt + (k_2 + k_3)\frac{D_2}{D_1} \int \frac{D_2}{D_1} q_{L1} dt$$

Note that the time dependence of control input $\frac{D_2}{D_1}$ in the integral terms prevents expressing (8) as an equivalent second-order system through the usual change of variable. Figure 2.2 depicts the operation of the system in Mode 1; therefore, the corresponding derivation of (8) is also done for Mode 1. The system in Mode 2 would yield similar equations and the SISO nature would remain unaltered.

The input control variable shown by the analytical analysis of this system is a ratio of two independent inputs, D_1 and D_2. This translates to a non-uniqueness whereby an infinite number of combinations of D_1 and D_2 exist such that the speed of the cab is adequately controlled. This also implies that, should one of the PMs have a fixed displacement, the system remains completely controllable within a finite range of speeds. This, together with the two modes introduced previously, results in a flexible architecture with many choices for control and operation design.

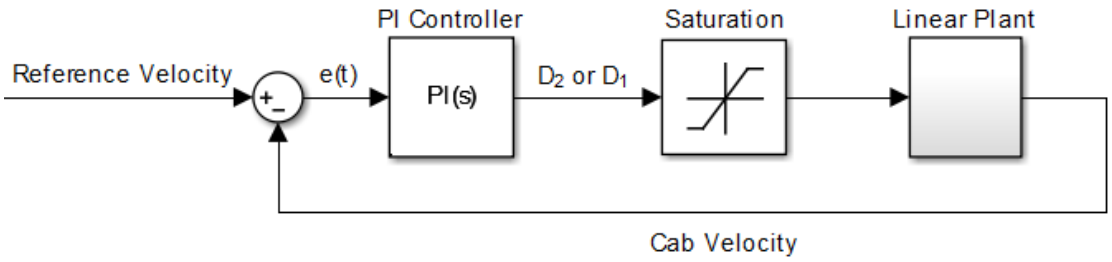

Figure 2.3: Block diagram of PM controllers as applied to the linear model

Although the linear model described by (8) does not capture the non-linearity inherent to the hydraulic system, it remains useful in the determination of preliminary control strategies. In this case, using (8), a linear simulation of the system is built using Matlab's Simulink environment wherein the input to the plant is either D_1 or D_2 (while the other holds constant) and the output is the load velocity. This allows for the design of preliminary proportional-integral (PI) linear feedback controllers used to control the displacements of the PMs. The controller gains determined in the preliminary design are then tuned as needed to ensure appropriate operation of the non-linear model, introduced in the next section. Characteristic to the feedback PI controller, the command signal generated depends on the error signal $e(t)$, as defined in Figure 2.3, and is of the form,

$$D_n(t) = P_n e(t) + I_n \int e(t)dt \tag{9}$$

where $n = 1,2$ to refer to the corresponding PM (PM_1 or PM_2) and P and I denote controller gains. The command signal $D_n(t)$ passes through a saturation block to limit minimum and/or maximum values of the signal as needed; the use of these saturation blocks will be further explored in the next section in the context of efficiency.

2.2.2 Control and Efficiency Considerations

To test the control efficacy and to determine the system's energy efficiency, a high-fidelity numerical model of the system is built using Matlab's Simulink/Simscape

environment [25], as depicted in Figure 2.4. Using the SimHydraulics tools within Simscape, the model incorporates the non-linearities neglected in the linear model by using the provided hydraulic component building blocks. Furthermore, functionality for the testing of various scenarios is also built in, such as a varying load (i.e., passengers), varying load travel heights, varying travel speeds, etc.

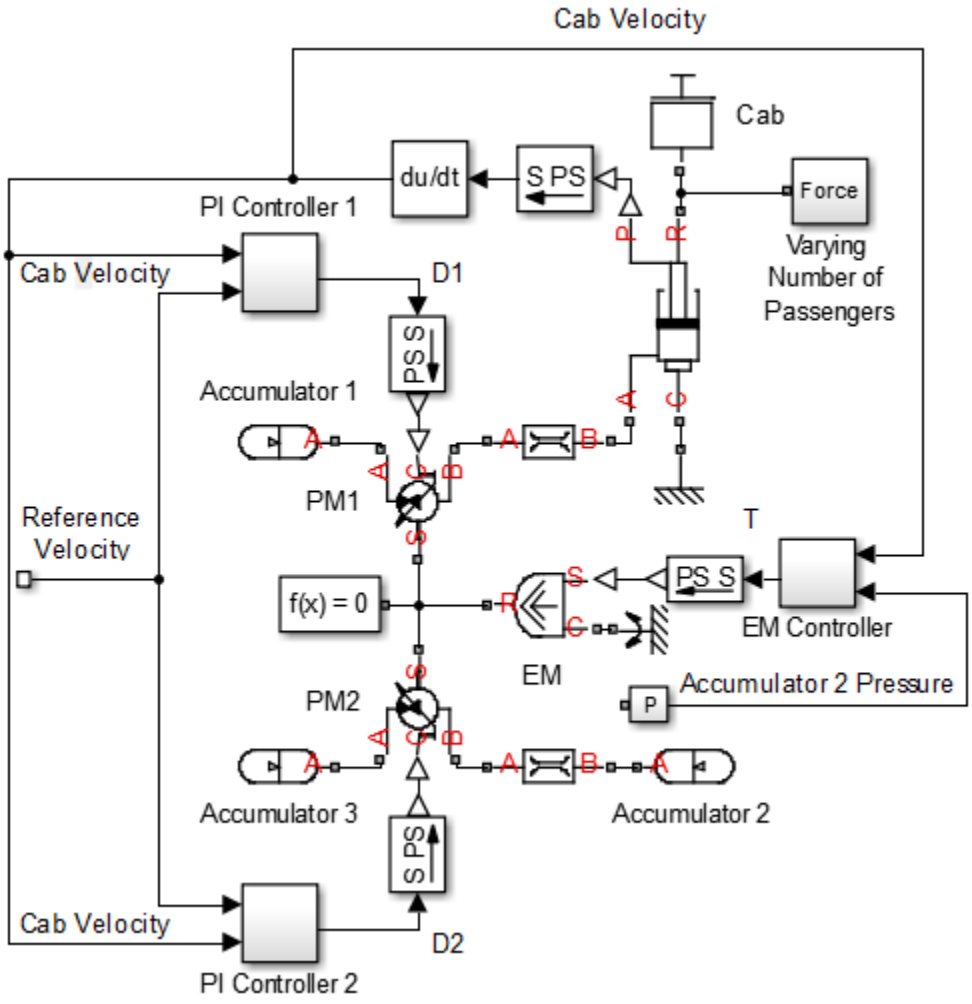

Figure 2.4: Simulink/SimScape hydraulic elevator model

The numerical model uses the built-in (nonlinear) SimScape gas-charged accumulator block for Accumulators 1, 2, and 3, and the SimScape variable-displacement hydraulic machine block to model the PMs. The losses in the system arising from hydraulic flow

are modeled using non-linear hydraulic resistances, as shown, for each fluid domain. Finally, an ideal torque source block models the EM.

The variable-displacement hydraulic machines take as inputs a control signal for their displacements D_1 and D_2 generated via (9) and saturated so as to limit the maximum value of the signal to the maximum attainable value of displacement for the corresponding PM. Additionally, $D_1(t)$ is also limited to a minimum displacement command, thereby giving preference to commanding PM_2, which ensures a more efficient operation, explained in detail later. Prior to reaching the SimScape block, the saturated signals coming from PI controllers 1 and 2, in Figure 2.4, are processed through the *SPS* blocks shown; the *SPS* blocks take a *Simulink* signal and convert it into a *Physical* signal able to be used by the SimScape variable-displacement hydraulic machine block.

The EM overcomes parasitic losses and compensates for energy temporarily lost by people ascending and then exiting the cab. In detail, the EM provides input energy during the descent of the cab while its output is suppressed during the ascent. This is done by feeding the cab velocity back into the EM and suppressing its output when the cab velocity is greater than zero (during ascent). A controller of the form of (9) again governs; however, the integral component is eliminated, which serves to avoid integrator windup during the time the controller output is suppressed. The EM compensates for any energy loss in the system; it does so by ensuring that enough energy (expressed as a fixed reference pressure) in Accumulator 2 always remains to drive a full cab back up to the top floor. This initial heuristic control strategy described was decided upon after assessing the efficiency of several possible control strategies, the process of which will now be described.

The system has four basic Control Operations: 1) using Mode 1, wherein Accumulator 2 provides power to lower the cab, while primarily controlling on D_1, 2) using Mode 1 while primarily controlling on D_2, 3) using Mode 2, wherein Accumulator 2 provides power to raise the cab, while primarily controlling on D_1, and 4) using Mode 2 while primarily controlling on D_2. To determine which operation to pursue, a simple analysis of the total system energy is performed. In Mode 1, for a given cab gravitational potential energy E_{cab}, the energy provided by Accumulator 1 (E_1) needs to both lift the cab and store sufficient energy E_2 in Accumulator 2 to return the cab back down. In the absence of losses, and neglecting the energy storage capacity of the low-pressure accumulator (Accumulator 3), the relationship becomes (10), where E_{tot} is the total energy *transfer* through the system for a given E_{cab}.

$$E_{cab} + E_2 = E_1 = E_{tot} \tag{10}$$

In Mode 2, both the energy provided by Accumulator 1 plus the energy provided by Accumulator 2 must suffice to lift the cab, while on the return, the gravitational potential energy of the cab divides into Accumulator 1 and Accumulator 2. In the absence of losses, and neglecting the energy storage capacity of Accumulator 3, the relationship (11) follows.

$$E_1 + E_2 = E_{cab} = E_{tot} \tag{11}$$

Figure B1 can again be referenced for a visual representation of the energy flows described by (10) and (11). Comparing (10) and (11), it becomes apparent that for the same given cab energy required (i.e., E_{cab} in both equations), E_{tot} will be less in Mode 2. This translates into a lower net energy loss in Mode 2 than in Mode 1, which points to Control Operation 3) and Control Operation 4) as more desirable. To further narrow down to the most desirable Control Operation, a closer look at the individual energy transfer of each PM is considered.

A variable displacement PM tends to have a reduced efficiency at small displacements [26]. This implies that in Control Operation 3), PM_1 operates less efficiently, while in Control Operation 4), PM_2 operates less efficiently. While PM_2 transfers only the energy flowing in and out of Accumulator 2, PM_1 transfers both the energy associated with Accumulator 1 and that associated with Accumulator 2. From this one can conclude that controlling on D_2 will result in lower net energy loss than controlling on D_1, and therefore Control Operation 4) emerges as the most desirable.

Within Control Operation 4), further necessary choices arise due to the non-uniqueness posed by the presence of controllable D_1 and D_2. One reasonable choice controls exclusively on D_2 while setting D_1 to ensure that PM_1, which transfers the most energy and thus subjects the system to its greatest losses, operates at its highest efficiency. A second choice controls both D_1 and D_2 using efficiency considerations of each PM. While this choice results in lowering of the operating efficiency of the high-energy transferring PM_1, large gains can be achieved in the operating efficiency of PM_2, potentially resulting in an overall higher system efficiency than had just D_2 been controlled. Additionally, increasing the displacement at which PM_2 operates can mitigate some of the noise associated with operating a PM at low displacements [27]. To determine which choice results in better efficiency, a detailed analysis of the operating efficiency of the PM's becomes necessary. Note that in Chapter 3 addresses the optimal control problem in which no *a priori* strategy is assumed for control of D_1 and D_2, and instead techniques such as Dynamic Programming are used, together with a given load cycle, to determine optimal trajectories of D_1 and D_2 through the control space.

To begin, the losses in a PM are characterized as a function of the differential pressure across the PM, the displacement of the PM and the angular velocity of the shaft. The losses can generally be described as losses due to leakage (volumetric losses), q_L,

which tend to account for large parts of the inefficiency [28], and losses due to friction of rotation (mechanical losses), T_{fr}, both of which are approximated by the following equations, given by [29], and incorporated into the appropriate simulation blocks of the SimScape model.

$$q_L = D\omega k_{L1}\left(\frac{\Delta P}{\Delta P_{nom}}\right)^{k_{LP}}\left(\frac{D}{D_{max}}\right)^{k_{LD}}\left(\frac{\omega}{\omega_{nom}}\right)^{k_{Lm}} \tag{12}$$

$$T_{fr} = D\Delta P k_{F1}\left(\frac{\Delta P}{\Delta P_{nom}}\right)^{k_{FP}}\left(\frac{D}{D_{max}}\right)^{k_{FD}}\left(\frac{\omega}{\omega_{nom}}\right)^{k_{Fm}} \tag{13}$$

In these relationships all k coefficients are empirically derived through testing of the PM unit. Here, the values of k are experimentally determined for an Eaton/Linde Duraforce PM as reported in [30].

The PM also has mutually exclusive modes of motoring and pumping. The efficiency of the unit as a function of the losses (leakage and friction) differs for both modes. Equations (14) and (15) encompass the effect of the different modes. The variable n differentiates the motoring mode ($n = -1$) versus the pumping mode ($n = 1$),

$$q = D\omega - nq_L \tag{14}$$

$$T = D\Delta P + nT_{fr} \tag{15}$$

thus the volumetric efficiencies in both the pumping and motoring mode, η_{mp} and η_{mm}, and the mechanical efficiencies in both the pumping and motoring mode, η_{vp} and η_{vm}, become,

$$\eta_{mp} = \frac{D\Delta P}{D\Delta P + T_{fr}}\ , \eta_{mm} = \frac{D\Delta P - T_{fr}}{D\Delta P} \tag{16}$$

$$\eta_{vp} = \frac{D\omega - q_L}{D\omega} \ , \eta_{vm} = \frac{D\omega}{D\omega + q_L} \tag{17}$$

In each mode, the total efficiency results from the product of both the volumetric efficiency and the mechanical efficiency. Finally, the dependence of the PM efficiency on three operating variables ($D, \omega,$ and ΔP) warrants some simplifications. Figures B2 and B3 in Appendix B provide the efficiency contours of the PM while holding displacement constant and differential pressure constant, respectively. From these two figures one can conclude that the PM efficiency varies little with changes in angular velocity. In light of this, for a particular operation, maintaining a constant ω and examining the efficiency as the other two variables vary satisfactorily describes the efficiency of the PM.

Equations (12) - (17), together with the simplification of holding ω constant, are used to examine the efficiency of both PM's while either a) D_2 is exclusively controlled, or b) both D_1 and D_2 are controlled. Table A2.1 in Appendix B provides the parameter inputs for the nonlinear model depicted in Figure 2.4, including the pertinent values for the reference motion profile and the reference pressure signal. Simulations are performed which extend the actuator a distance of 14.6 m and retract it the same amount, under a load of 2080 kg. Figure 2.5 depicts the operating points for the PM's using both control strategies to achieve this movement. Note that contours indicate PM efficiency. When controlling exclusively on D_2, PM_1 operates most efficiently (since it maintains its maximum displacement); however, PM_2 reaches an efficiency as low as 70%. Alternatively, controlling both displacements allows for significant improvements in the operating efficiency of PM_2 at the cost of a lower operating efficiency of PM_1. Due to this inherent tradeoff, the control approach which yields greater efficiency requires further evaluation.

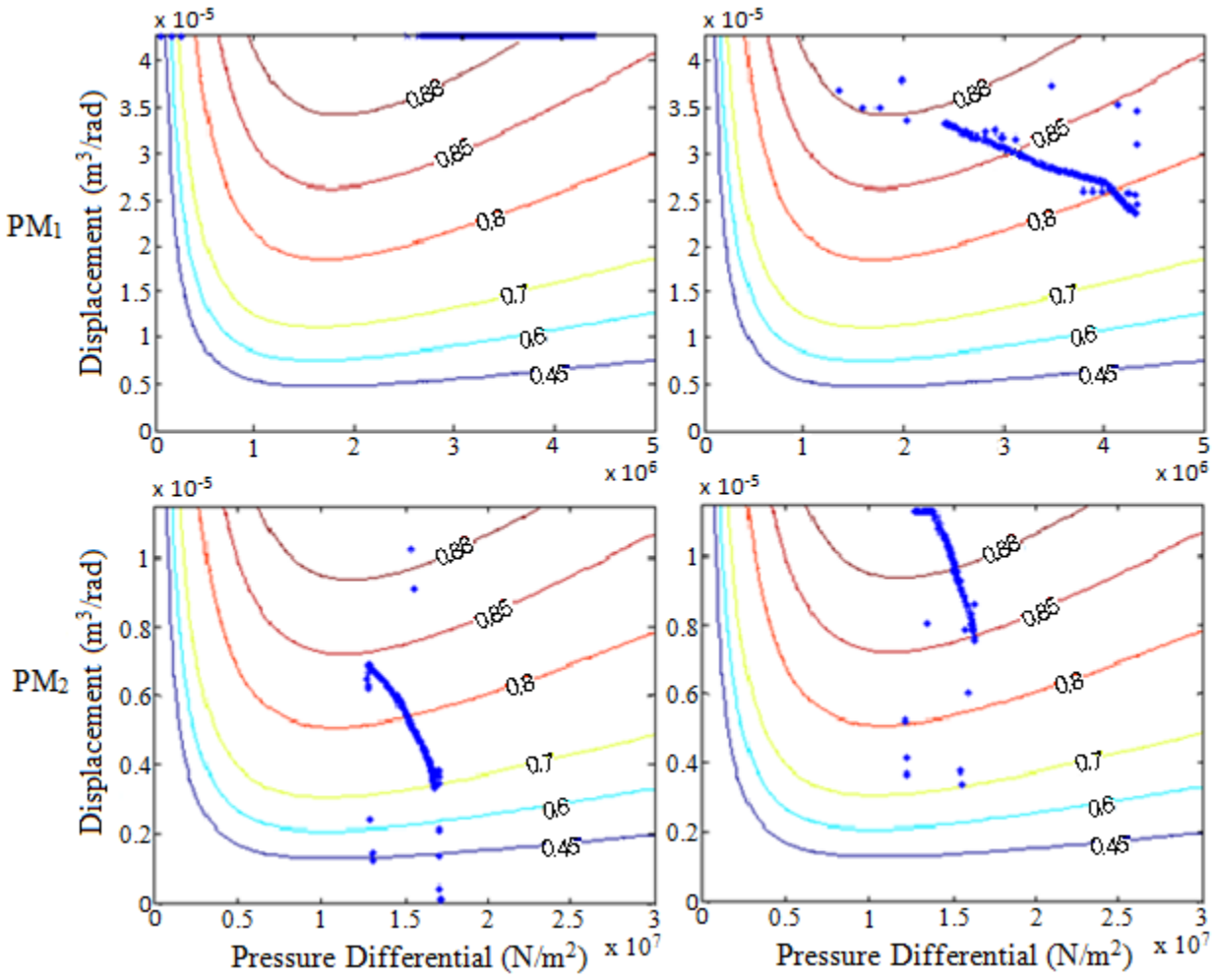

Figure 2.5: Contrast of operating regions of each PM when only PM_2 displacement is controlled (left subfigures) and when both PM_1 and PM_2 displacements are controlled (right subfigures).

For a typical hydraulic elevator, an analysis of the total actuation efficiency of the system (calculation is described in detail in Section 2.3) with both control strategies is shown in Figure 2.6. Here, one can clearly see improvement in efficiency when controlling on both D_1 and D_2, particularly when the cab carries a lower payload.

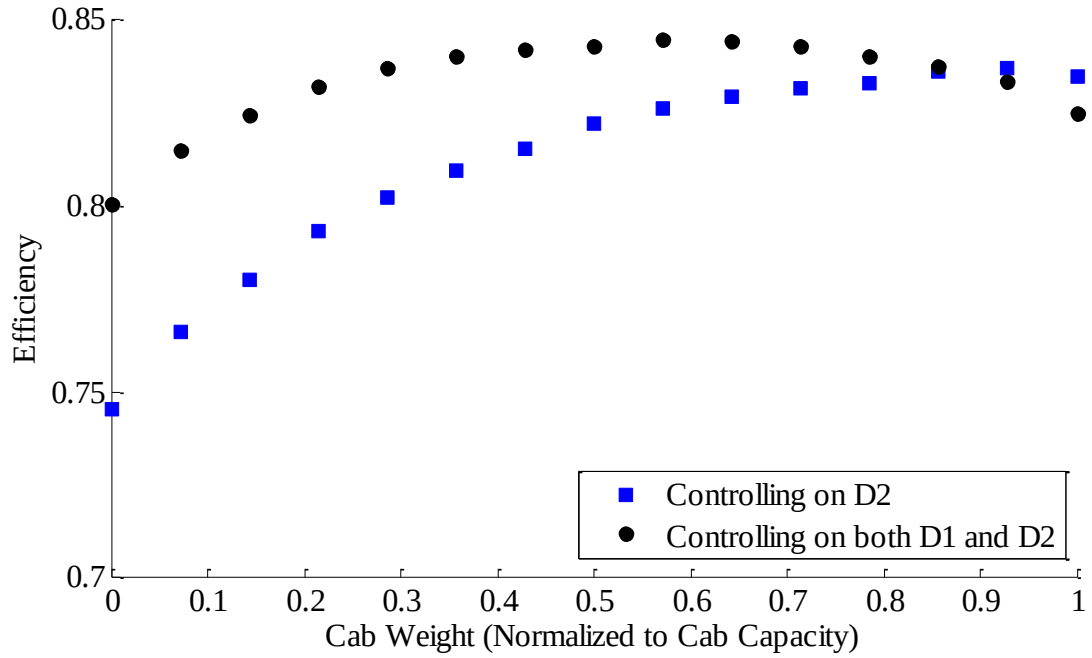

Figure 2.6: Comparison of control strategies as pertains to actuation efficiency.

These results allowed the design of the final heuristic control strategy: control on both D_1 and D_2 wherein higher authority is given to D_2 control by limiting the minimum value of the D_1 control signal. This ensures that PM_1, which transfers the most energy, does not operate below a minimum efficiency. It should be noted, that while the control strategy developed here incorporates key efficiency characteristics of the system, it serves only as a preliminary strategy as it lacks more rigorous insight such as that given by DP in Chapter 3.

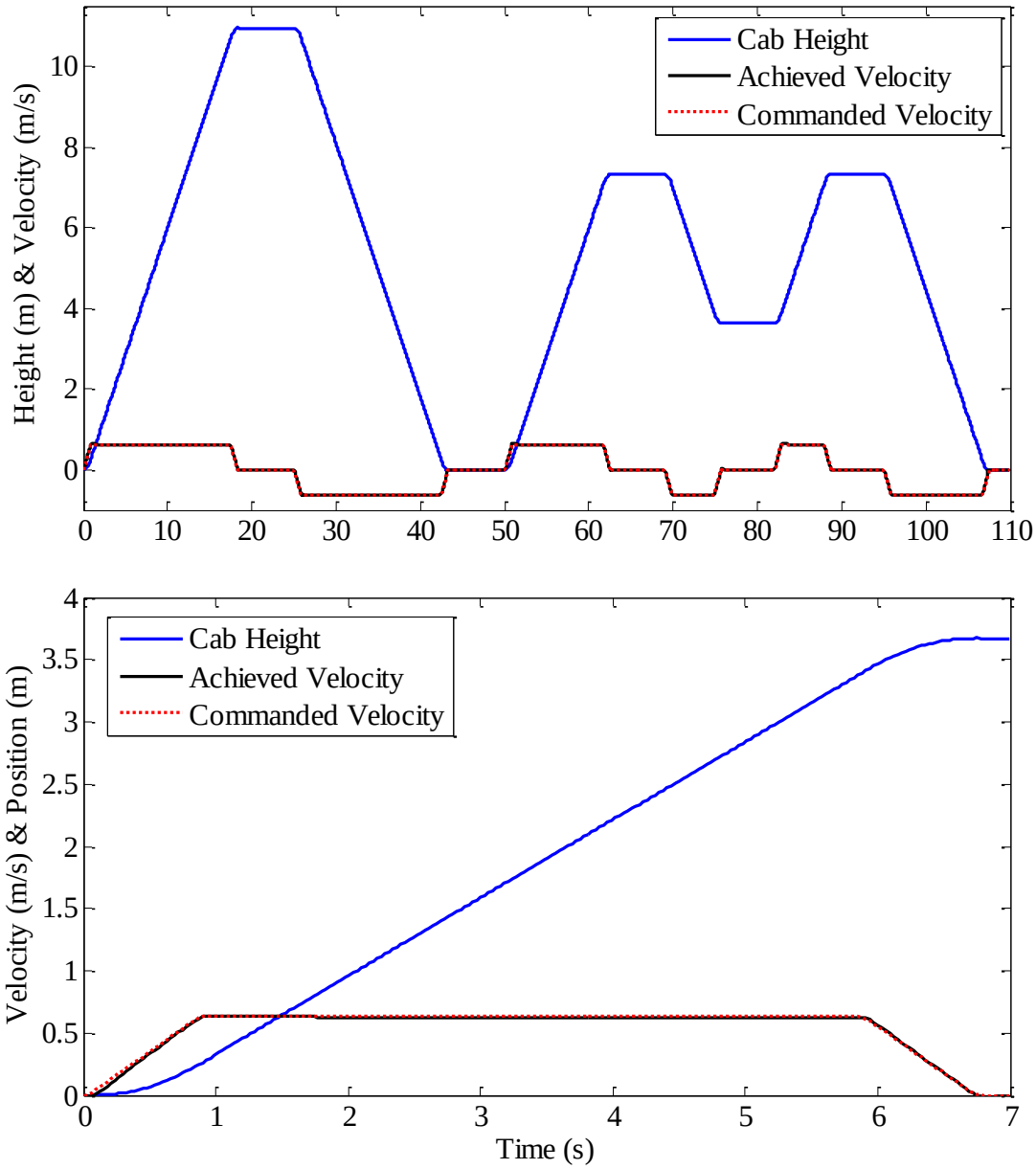

Figure 2.7: Simulation results for the introduced architecture controlled for velocity through a schedule of floors (top); details of simulated motion moving up through a single floor (bottom).

Figure 2.7 depicts output from the nonlinear simulator displaying the ability of the architecture and the selected control strategy to accurately position the load through a given schedule of floors (4^{th}-1^{st}-3^{rd}-2^{nd}-3^{rd}-1^{st}) using a desirable velocity profile and a load

of 2080 kg (corresponding to a full elevator cab). The bottom subfigure depicts simulation results for commanded and obtained velocity as the cab moves up through a single floor. Note that these results provide evidence that the elevator system successfully navigates the schedule of floors while the control strategy accurately tracks the reference velocity profile.

2.3 Efficiency and Energy Consumption Comparison

An efficiency comparison of both the system introduced herein, heretofore referred to as the present system in this chapter, and a recent electrohydraulic system [19, 20] depicted in detail in Figure A1 allows one to assess the performance and merits of the present system as compared to a concept shown to be preferable over contemporary methods. The electrohydraulic system incorporates a bi-directional pump/motor driven by an electric machine (EM) with both generator and motoring functionality. The EM siphons off power from the system when the direction of flow is from a high pressure to a low pressure, which is then either fed back to the grid or stored in a battery. When the direction of flow is from a low pressure to a high pressure the EM provides power to the system from the grid or the battery. Figure B4 in Appendix B depicts a SimScape model built for the electrohydraulic system. The components shared by both systems are sized identically so as to ensure comparability. Table B2 in Appendix B tabulates the system parameters, including the EM controller; the present system uses the parameters previously tabulated in Table B1.

The actuation efficiency of both systems is calculated at each payload level, ranging from an empty cab (1100 kg) to a full cab (14 people, 2080 kg); an average of 70 kgs is used per person. 15 simulations are performed, one for each payload level, of the cab traveling to the 4^{th} floor and returning back down. The total system actuation efficiency,

governed by the individual efficiencies of the components, is calculated as a ratio of energy recovery (E_{out}) to energy expenditure (E_{in}). The energy storage capacity of Accumulator 3 is again neglected as well as energy losses associated with Accumulators 1 and 2. Energy losses in hydraulic accumulators are primarily due to the heat exchange that occurs between the gas and the pressure vessels; in much less measure, friction losses within the accumulator also contribute. A properly designed accumulator can severely mitigate heat exchange losses and achieve an efficiency rating of up to 95% [31].

For the present system during ascent, E_{in} is primarily provided by Accumulator 1 and Accumulator 2 while the gravitational potential energy stored in the cab (E_{cab}) is used for E_{out}. Thus, the total efficiency of the system when the cab ascends follows as,

$$\eta_{system1} = \frac{E_{out}}{E_{in}} = \frac{E_{cab}}{E_1 + E_2} \tag{18}$$

During descent, the auxiliary EM will begin to input energy into the system, the gravitational potential energy adds to this input, while the output energy is that entering both accumulators through the descent. The efficiency of the system while descending then follows as,

$$\eta_{system1} = \frac{E_{out}}{E_{in}} = \frac{E_1 + E_2}{E_{cab} + E_{EM}} \tag{19}$$

In the electrohydraulic system, an accumulator, operating as the hydraulic counterweight, acts as a continuous power source to the cab. An electric machine coupled with a PM adds or subtracts power as needed to maintain a desired velocity profile. In the case where energy is subtracted, a battery stores the energy and later returns it to the system. The efficiency of the accumulator associated with this system is also neglected so as to maintain comparability. The energy conversion efficiency of the

battery, $\eta_{battery}$, conservatively estimated at 75%, applies both when charging and depleting the battery.

On the ascent, E_{in} in the electrohydraulic system equals energy provided by its accumulator, the EM, and the battery, while E_{out} is the gravitational potential energy.

$$\eta_{system2} = \frac{E_{out}}{E_{in}} = \frac{E_{cab}}{E_{accumulator} + E_{EM} + E_{battery}} \tag{20}$$

On the descent, E_{in} is the gravitational potential energy while E_{out} equals the energy into the accumulator plus the energy supplied to the battery.

$$\eta_{system2} = \frac{E_{out}}{E_{in}} = \frac{E_{accumulator} + E_{battery}}{E_{cab}} \tag{21}$$

The energy leaving or entering an accumulator over time is determined by the time integral of the product of the pressure and flow through the pressure node associated with the accumulator, or:

$$E_{accumulator} = \int Pqdt \tag{22}$$

Similarly, the energy provided by the EM is the integral of the product of its torque T, and its speed ω given by:

$$E_{EM} = \int T\omega dt \tag{23}$$

The ideal torque source employed to model the EM does not capture the loss characteristic of an EM; because of this, post processing of the results incorporates the losses. The losses of an electric motor in operation, as a function of the torque T, and the angular velocity of the shaft ω, are approximated by the following equation [32]:

$$P_{losses} = k_c T^2 + k_i \omega + k_\omega \omega^3 + C \tag{24}$$

These losses arise due to electrical resistance of the wires in the motor, $k_c T^2$, due to the magnetic effect on the iron of the motor, $k_i \omega$, due to friction and windage, $k_\omega \omega^3$, and due

to components of the motors that operate at all times, C. The different k coefficients and the value of C are generally provided by the manufacturer of the electric motor. This paper uses coefficients from those given in [32]. Using this relationship for losses the efficiency for the electric machine in both motor and generator modes can be calculated by (24) and (25), respectively, as follows:

$$\eta_m = \frac{P_{out}}{P_{in}} = \frac{P_{out}}{P_{out} + P_{losses}} = \frac{T\omega}{T\omega + k_c T^2 + k_i \omega + k_\omega \omega^3 + C} \tag{25}$$

$$\eta_g = \frac{P_{out}}{P_{in}} = \frac{P_{in} - P_{losses}}{P_{in}} = \frac{T\omega - k_c T^2 - k_i \omega - k_\omega \omega^3 - C}{T\omega} \tag{26}$$

where P_{out} represents power output and P_{in} represents power input of the EM.

Using (18)-(26), a complete analysis of the actuation efficiency is performed. Pressures, flows, torque, shaft speed, cab height, and cab velocity are all recorded throughout simulations. Figure 2.8 reports the actuation efficiency as it varies with the cab payload for both systems.

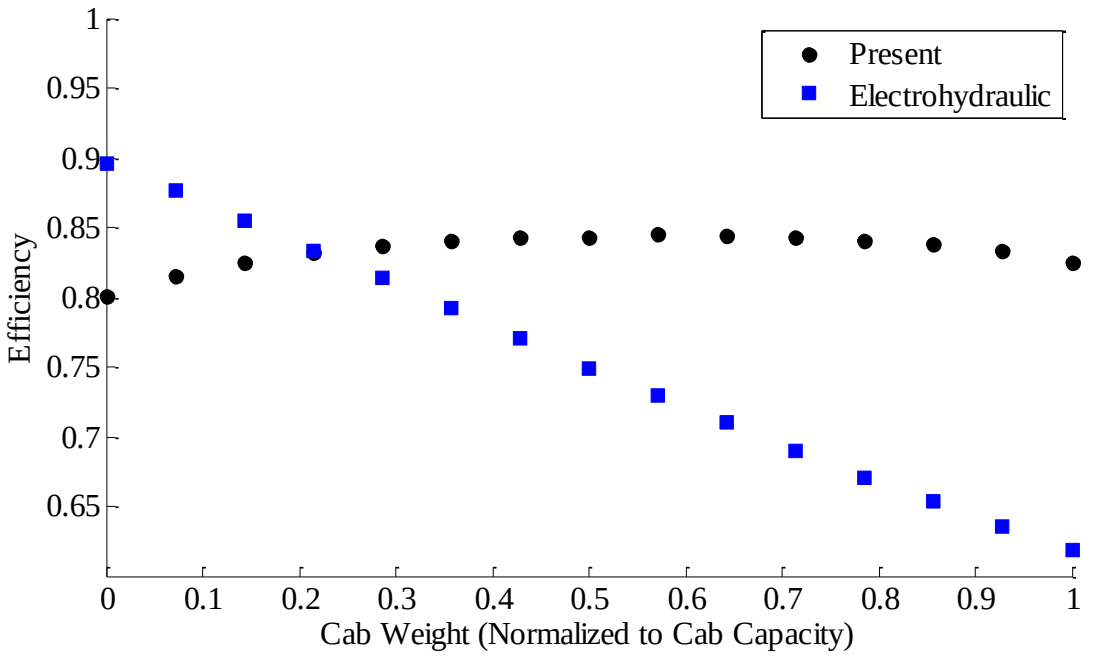

Figure 2.8: Efficiency during operation as a function of cab load

With an empty cab, the electrohydraulic system has higher actuation efficiency. This high efficiency results from a low participation of the EM since the accumulator provides the majority of the energy during actuation. However, when the cab weight reaches approximately one fifth of its maximum weight (corresponding to 3 people in the cab), the present system begins to gain an advantage, improving by up to 13% when the cab carries a full payload.

While the efficiency of actuation proves useful, the typical elevator consumer makes purchasing decisions based more on the net energy (and its cost) usage for a given system. A discussion of the energy usage characteristics from the present architecture is first realized before providing a comparison between it and the electrohydraulic system. Figure 2.9 depicts the pressure of all accumulators in the present architecture while the simulator moves 50 persons.

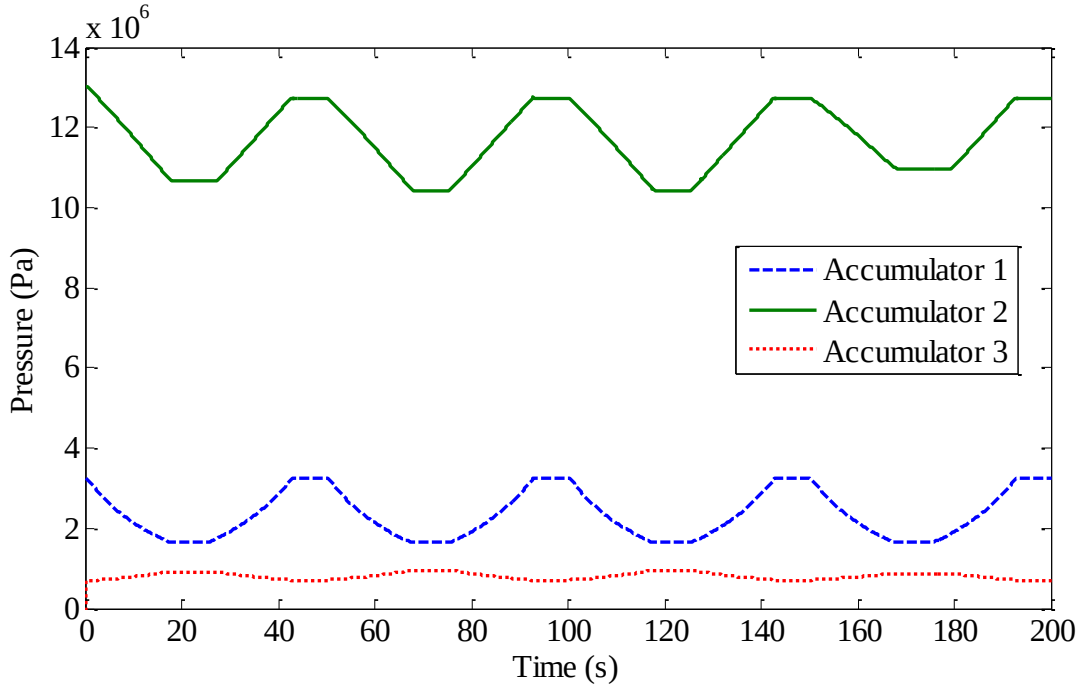

Figure 2.9: Accumulator pressures in the system while 50 people are brought up to the 4th floor; full cab capacity.

In the figure, the cab performs four trips to bring the 50 persons up to the 4th floor. A trip here refers to the cab going up to the desired floor and then returning to the ground floor. Should people be descending, the cab ascends empty (1100 kg), and descends with the specified load. Should people be ascending, as is the case in Figure 2.9, the cab ascends with the specified load and descends empty. To bring 50 people up to the 4th floor, the cab performs three trips while carrying 14 persons, and one trip while carrying 8. As per the designed operation of the system, Accumulator 2 depletes while the cab ascends, and recharges using the cab potential energy and the EM when descending. The EM ensures that Accumulator 2 always reaches a desired pressure when the cab is fully down, as can be seen in the figure. Note that on the last trip the pressure drop of Accumulator 2 is noticeably less than the other three. This occurs since on the fourth trip, the elevator only carries 8 persons up, and therefore Accumulator 2 releases less

energy. This also translates into less energy input from the EM since the energy lost from 8 people ascending is less than that from 14 people ascending. It then follows that an empty cab ascending to bring people down will require even less energy input from the EM. Figure 2.10 depicts such a scenario.

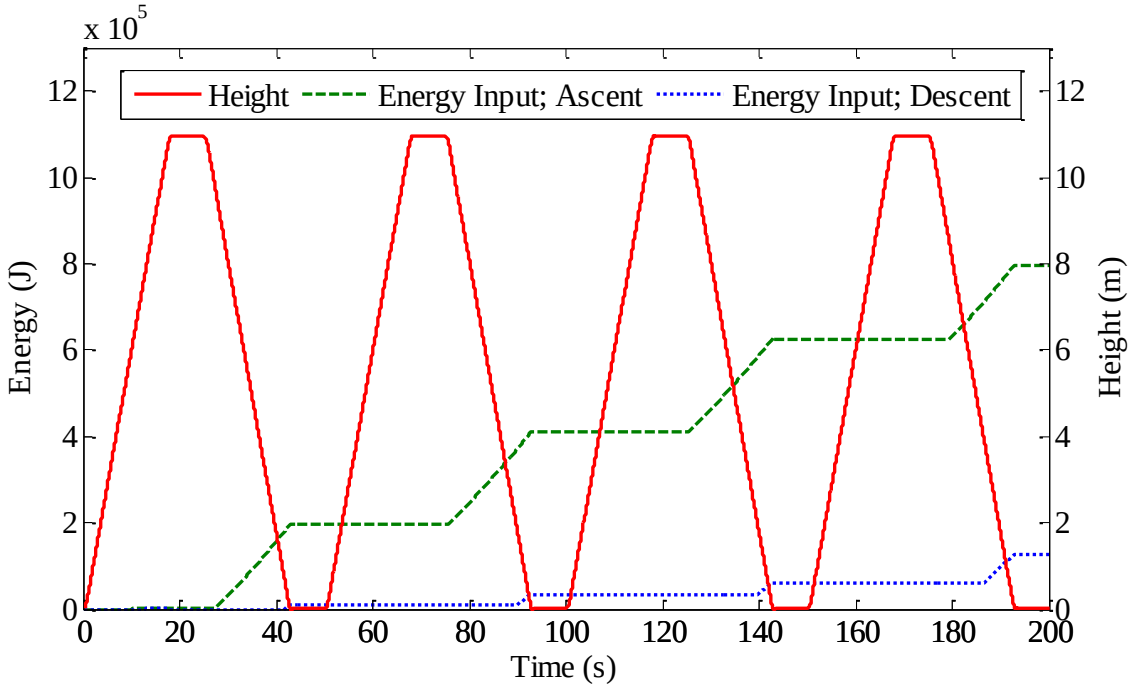

Figure 2.10: Energy input required to move 50 persons up (ascent) and 50 persons down (descent) from the 4th floor.

In Figure 2.10 the energy input into the system required to move 50 persons up to the fourth floor (ascent) is contrasted with that required to bring 50 persons down from the fourth floor (descent). Energy input is calculated from (23). In both cases, the cab executes 4 trips as described previously. Note that, as per the control strategy described previously, the energy input increases only during the descent of the cab (corresponding to periods of EM operation). From the figure, it becomes clear that people descending will require less energy input into the system. This introduces a characteristic of the system that results in a period of high energy consumption (people

ascending) and a period of low energy consumption (people descending); which may be favorable in some applications such as integrating the power supply with renewable power sources (photovoltaic cells) whose period of maximal power generation may coincide with periods of high energy consumption (i.e., commercial applications in which people ascend during daylight hours).

With the energy consumption characteristics of the system now described, a comparison (of the energy consumption) between the present system and the electrohydraulic system is now introduced. Recording the system energy input, E_{EM}, in both systems for a full day operation of the elevator provides the necessary data for the comparison. A full day for this comparison entails 50 persons, per floor, descending, and then ascending. Both of the systems are simulated in a four floor building, which implies a total of 150 persons being moved (1st floor is bottom floor). For a day's period, a minimum cab load (1 person) entails simulating the cab as it brings all 150 persons, up and down, one-by-one. Similarly, a full cab load (14 persons) entails the cab carrying 14 persons, unless there are less than 14 persons remaining on a floor, at which point the cab carries the remaining; this was introduced previously in the simulations performed for Figures 2.9 and 2.10. For easier reference, Figure B5 in Appendix B depicts a full day operation for a cab load of 13 people for one floor. With these definitions for a full day, the cab performs a total of 300 trips at its minimum cab capacity: 50 trips to move persons up and 50 trips to move them down for a total of 100 trips per floor beyond the 1st floor (bottom floor). Accordingly, at its maximum capacity the cab performs a total of 24 trips (8 per floor). Table B3 Appendix B tabulates the total trips for a full day at each cab load. It therefore follows that for both systems a minimum cab capacity, although actuated highly efficiently (electrohydraulic system), requires more net energy input than running a consistently full cab due to the larger number of trips required. Figure 2.11

depicts the daily energy input as a function of the cab weight (ranging from 1 person to 14 persons) used for the full day simulation, together with results for the electrohydraulic architecture.

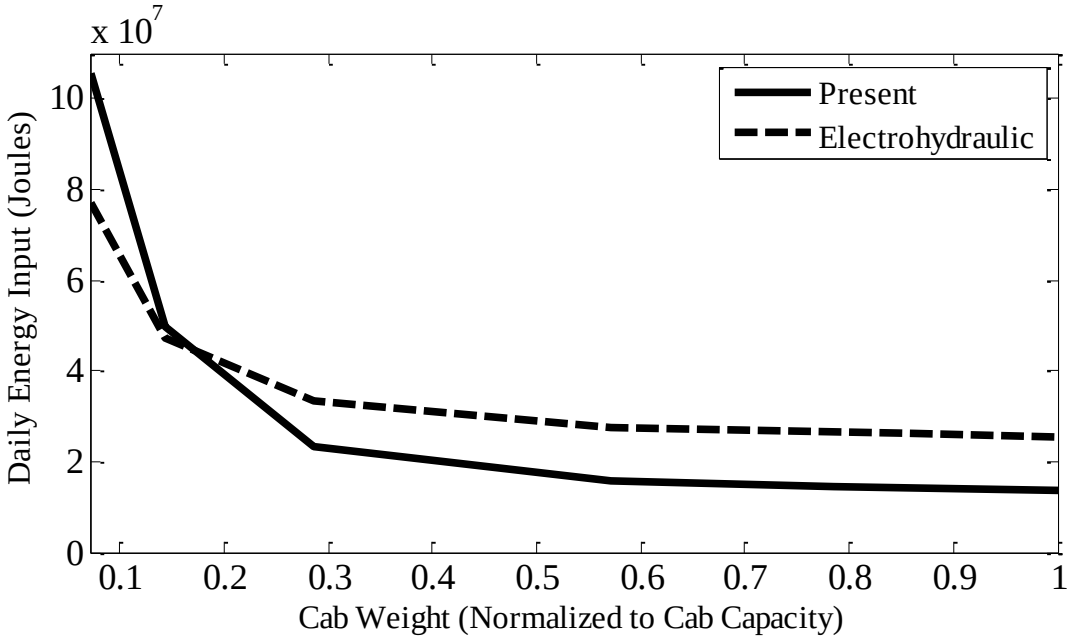

Figure 2.11: Daily input energy as a function of cab payload

Similar to the actuation efficiency results presented earlier, the present system tends to gain an advantage as the cab payload increases, reaching as high as a 23% reduction in daily input energy over the electrohydraulic system. The comparison of both systems yields results in favor of the present system introduced. For low occupancy rates, the present system falls short in both actuation efficiency and daily input energy; however, when the cab transports more than 2 or 3 people per trip, the present system gains advantages in both measures. Many elevator applications meet this condition, particularly in residential and commercial applications where the majority of the people traffic occurs at the beginning and end of the day. The present system also benefits from relative simplicity since it incorporates its own energy storage devices, as opposed

to the electrohydraulic system which requires power electronics and batteries, or a means to return electrical energy to the grid.

The comparison between the electrohydraulic system and the present system sought to identify the virtues of the present system when compared to the state-of-the-art in hydraulic actuation (electrohydraulic regeneration is common not only in elevators, but many hydraulic actuation industries [21, 22]). Nevertheless, conventional hydraulic actuation technologies have been slow to adapt to the emerging technology. It is pertinent therefore, for practical purposes, to perform a quick study on the merits of the present system as compared to a more commonly used throttling architecture. The schematic of one such architecture is shown in the inset of Figure 2.12. The daily energy consumption of the conventional architecture was calculated using the same procedure as described above with the simplifying assumptions, for the sake of speed, that the system operates at 100% efficiency and the cab regenerates no energy on descent; wherein the energy input into the system E_{EM} then simply becomes the required energy into the cab to reach the desired height. It should be noted that a throttling architecture does not in fact regenerate any energy and the assumption of 100% efficiency only underestimates the energy consumption of the throttle-based architecture.

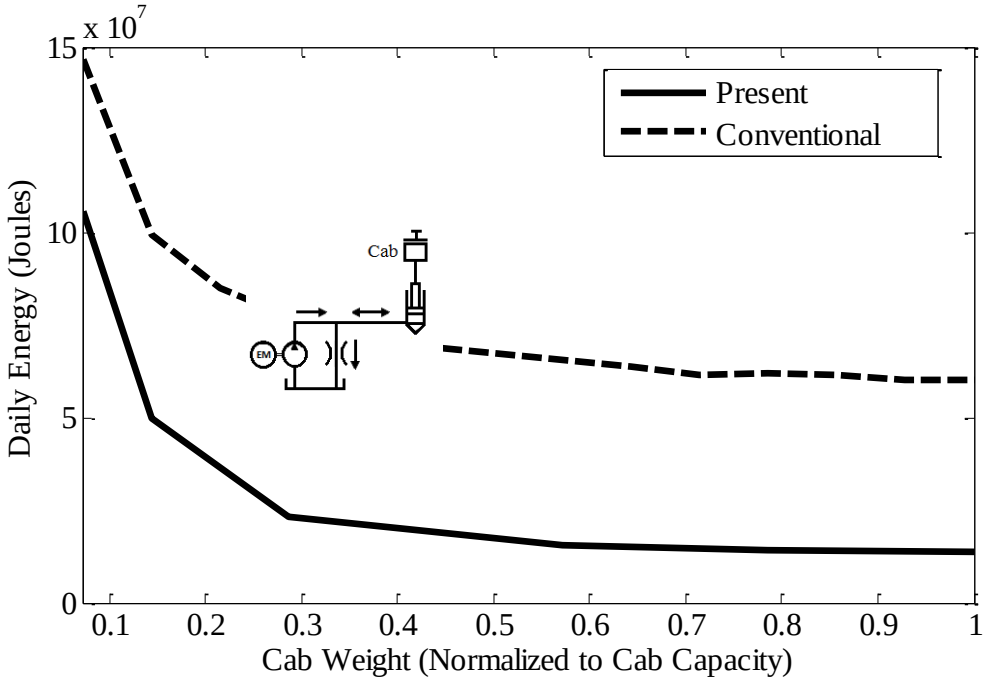

Figure 2.12: Daily energy consumption comparison; Present vs Conventional

Predictably, Figure 2.12 reports an upwards of 75% reduction in daily energy by using the present system as opposed to the conventional throttle-based system. Both this comparison and the comparison with the electrohydraulic system firmly establish the potential of the introduced novel hydraulic actuation architecture to improve upon the hydraulic actuation industry.

2.4 Summary

This chapter introduced a hydraulic architecture for speed control and energy regeneration in hydraulic actuation. The architecture is applied to hydraulic elevator. In the absence of losses, the system makes use of a specialized form of a hydraulic transformer to achieve a self-sufficient energy flow exclusively using pre-charged accumulators and provides functionality for motion control via variable displacement hydraulic pump/motors. Governing equations were derived for a simplified version of the

system, exposing non-uniqueness in the independent control. Exploitation of this non-uniqueness allowed for efficient control of the system using simple PI controllers. In practical application, the new architecture requires a small external power source (e.g., an electric motor) to overcome component losses. Simulation results using a high-fidelity, nonlinear simulator, demonstrate the effectiveness and efficiency of the architecture. In comparison to similar simulation results for a recently introduced electrohydraulic system, the introduced architecture exhibited up to a 13% increase in actuation efficiency and a 23% decrease in daily input energy over a typical usage cycle. Additionally, comparison to a more commonly used throttle-based architecture exhibits upwards of a 75% decrease in daily energy consumption. These results suggest that the new architecture may be attractive for continued exploration.

CHAPTER 3

OPTIMIZATION OF NOVEL HYDRAULIC ARCHITECTURE

3.1 Introduction

Chapter 3 of this thesis ventures beyond heuristic considerations for control and sizing of the introduced hydraulic architecture (as applied to an elevator). A preliminary sizing procedure is presented and the design degrees of freedom (DDOF) identified. DP-informed Monte Carlo simulations are performed to determine optimal values for the DDOF. Monte Carlo simulations yield a region of optimality within the space formed by the DDOF; accordingly, the final values for the component sizing are chosen. Characteristics of optimal control are determined through the employment of DP on a backward-looking simulation. DP is applied on the elevator undergoing three different load cycles, the result of which identifies two main characteristics of optimal architecture control: 1) the maximization of D_1 and 2) the use of the EM upon descent. A rule-based controller is then developed on a forward-looking simulation using the characteristics of optimal control determined. Energy usage from the forward-looking simulation is compared to that of DP and found to be 62% optimal. Energy usage from the DP-informed architecture is compared to that of the heuristically developed architecture in Chapter 2 and found to be 21% less. DP optimization process is then used on the hydraulic architecture a second time, now in the context of the hydraulic forklift. Sizing, optimal control, and rule-based control are all performed a second time. Energy usage from the resulting forward-looking simulation is compared to that of DP and found to be 51% optimal.

3.2 Optimal Sizing of Novel Hydraulic Architecture: Elevator

Fluid power system design often involves a repetitive process when attempting to properly size system components. The hydraulic circuit is generally simulated several times with changing parameters in an effort to narrow down component sizing such that the hydraulic circuit performs as required [33]. This quickly becomes a time-consuming process and very often yields multiple choices of component sizes which satisfy performance requirements; choices which then need to be narrowed down to that which performs, as required, "better" than the other possible choices. This most often translates to the choice which yields the most energy efficient operation.

The results shown in Chapter 2 demonstrate promise from the architecture; however the heuristic nature of the sizing failed to contemplate the "better" choices for component parameters. In this section, the gaps left by Chapter 2 with respect to sizing are closed. To this end a preliminary sizing procedure is developed and used alongside DP and Monte Carlo simulations to achieve a more rigorous sizing strategy.

3.2.1 Preliminary Sizing Procedure

Preliminary sizing of the hydraulic architecture uses motion and energy constraints specific to both the architecture and the application (elevator) to define many components of the system. Specifically, *a priori* motion and load parameters needed are: a_{max}, v_{max}, m_{max}, m_{min}, and h_{min}.

These parameters vary depending on the application of choice, as such, in the case of the elevator, the values for these parameters are defined accordingly (Table 3.1).

Table 3.1: Motion and load parameters for sizing procedure; Elevator

Parameter	Value
$\boldsymbol{a_{max}}\ \left(\frac{\boldsymbol{m}}{\boldsymbol{s^2}}\right)$	0.75
$\boldsymbol{v_{max}}\ \left(\frac{\boldsymbol{m}}{\boldsymbol{s}}\right)$	0.63
$\boldsymbol{m_{max}}\ (\boldsymbol{kg})$	2080
$\boldsymbol{m_{min}}\ (\boldsymbol{kg})$	1100
$\boldsymbol{h_{max}}\ (\boldsymbol{m})$	7.3

Additionally, the elevator in this section uses a cab capacity of 14 people averaging 70 kg each, in a 3-floor building (hydraulic elevators are mainly low-rise). Limiting the number of floors helps mitigate long computational times associated with DP.

The sizing procedure starts with the actuator. The hydraulic cylinder is defined by the area, A_{req}, which is needed such that the rated pressure of the cylinder, P_{cmax}, is not surpassed. The constraint for the area of the cylinder is therefore expressed as follows,

$$A_{req} \geq \frac{m_{max}(a_{max} + g)}{P_{cmax}} \tag{27}$$

An established area, A, of the cylinder constrains a minimum fluid volume required by Accumulator 1 such that there is enough fluid available in the top fluid domain to fully extend the actuator. This is given by,

$$V_{1fluid} \geq A * h_{max} \tag{28}$$

Similarly, the maximum operating pressure of Accumulator 1, P_{1max}, can be constrained by ensuring that P_{1max} is never higher than the minimum pressure on the cylinder side.

$$P_{1max} \leq \frac{m_{min} g}{A} \tag{29}$$

Furthermore, the energy stored by Accumulator 1, U_1, at its maximum operating pressure can also be constrained such that it holds just enough energy to lift an empty cab to maximum extension.

$$U_1 \leq m_{min} * g * h_{max} \tag{30}$$

The constraints for both U_1 and P_{1max} allows PM_1 to be exclusively used for pumping during cylinder extension and exclusively used for motoring during cylinder retraction; a mode of operation that was found to be preferable in Chapter 2.

Assuming adiabatic expansion and compression of gas, and given the constraints above, a value for the pre-charge pressure of Accumulator 1, P_{1pr}, can be found using the following relationship,

$$V_{1fluid} - \frac{0.4U_1\left(1 - \left(\frac{P_{1pr}}{P_{1max}}\right)^{\frac{1}{1.4}}\right)}{\left(\left(\frac{P_{1max}}{P_{1pr}}\right)^{\frac{0.4}{1.4}} - 1\right)P_{1pr}} = 0 \tag{31}$$

thereby fully defining Accumulator 1. Finally, the remaining component of the top fluid domain is sized by considering that a maximum flow of q_{1max} is required from PM_1. The area of the actuator, together with the maximum velocity, constrain the size of PM_1 as such,

$$q_{1max} = v_{max} * A \tag{32}$$

$$D_1 = \frac{q_{1max}}{\omega} \tag{33}$$

where ω is the maximum shaft speed experienced throughout operation. ω can be chosen considering the nominal shaft speed of the family of PMs under consideration, however it remains a fairly flexible DDOF in the sizing procedure.

The bottom fluid domain consists primarily of Accumulator 2 and PM_2. Accumulator 2 is sized such that it will store a certain required energy U_2 that responds to the application. In the hydraulic elevator, Accumulator 2 will need to store the energy equivalent of each floor full of people. This is because conceivably multiple trips of full cabs descending are possible while the cab remains empty during ascent (evening traffic in commercial applications) thereby providing Accumulator 2 with more energy than it releases. By convention, an average of 50 people per floor is considered. Consequently, the expression for U_2 can be expressed by,

$$U_2 = \sum_{f=1}^{3} h_f m_{person} g P_{floor} \tag{34}$$

where m_{person} is the average mass of a single rider, P_{floor} is the amount of people per floor, and h_f is the height of the floor corresponding to $f = 1,2,3$. With U_2 defined, the size of Accumulator 2, expressed as its volume capacity, can be found by,

$$V_2 = \frac{0.4U_2}{\left(\left(\frac{P_{2max}}{P_{2pr}}\right)^{\frac{0.4}{1.4}} - 1\right)P_{2pr}} \tag{35}$$

where P_{2pr} is the pre-charge pressure and P_{2max} is the maximum operating pressure. Both P_{2pr} and P_{2max} are also fairly flexible DDOF that when chosen still allow the energy constraint U_2 to remain met. Moreover, the separated nature of the fluid domains

maintains P_{2max} free from the constraint imposed by P_{cmax} allowing for higher Accumulator 2 pressures to be used, thereby reducing its size.

Accumulator 3 is defined by Accumulator 2. Similar to Accumulator 1, Accumulator 3 is limited to a maximum operating pressure, P_{3max}, that stays below that of Accumulator 2, so as to ensure operation of PM_2 in the right modes.

$$P_{3max} \leq P_{2max} \tag{36}$$

The pre-charge pressure of Accumulator 3, P_{3pr}, is then iterated through so as to define a minimum capacity V_3 such that a minimally-sized Accumulator 3 is achieved. The relationship between P_{3pr} and V_3 is as follows,

$$V_3 = \frac{V_{2fluid}}{1 - \left(\frac{P_{3pr} + Pa}{P_{3max} + Pa}\right)^{\frac{1}{1.4}}} \tag{37}$$

where Pa is the value of atmospheric pressure. (37) ensures that Accumulator 3 is capable of holding all the fluid expelled from Accumulator 2 while still maintaining its pressure constraints.

Finally the resulting size for PM_2 is considered using a torque balance between it and PM_1 such that a minimal pressure differential in the bottom fluid domain can still motor a large pressure differential in the top fluid domain, as follows,

$$D_2 = \frac{\left(P_{cmax} - P_{1pr}\right)D_1}{P_{2pr} - P_{3max}} \tag{38}$$

3.2.2 DP-informed Monte Carlo Sizing

The preliminary sizing procedure discussed in Section 3.2.1 identified three DDOF. These parameters, ω, P_{2pr}, and P_{2max}, considerably influence the overall efficiency of

the system. Therefore, the resulting problem then entails finding optimal values for these DDOF which result in higher efficiencies. One method of solving this problem is through the use of DP-informed Monte Carlo Simulations. Monte Carlo simulations rely on repeated random sampling to obtain numerical results [34]. In general, they follow a particular pattern which consists of: 1) Defining a domain of possible inputs, 2) generating inputs randomly from a probability distribution over the domain, 3) performing a deterministic computation on the inputs, and 4) aggregating the results.

The application of this procedure in the context of the hydraulic architecture contemplated within is discussed next. The three-dimensional design space formed by the DDOF constitutes the domain, over which Matlab capabilities are used to randomly generate values of the DDOF under a uniform probability distribution. DP then provides a deterministic computation on the input. As is discussed in detail in the next section, given a predefined motion profile (Figure 3.1), DP will yield an optimal control path for the system resulting in a minimum value for the energy usage throughout the specified motion. In this way, for unchanging values of the DDOF, DP always yields the same minimum value of energy usage; thereby rendering the computation deterministic such that repeated computations with random values over the domain allows for the specification of a region within the domain in which energy usage would be minimum. This region defines the values of the DDOF and therefore the optimal sizing of the system.

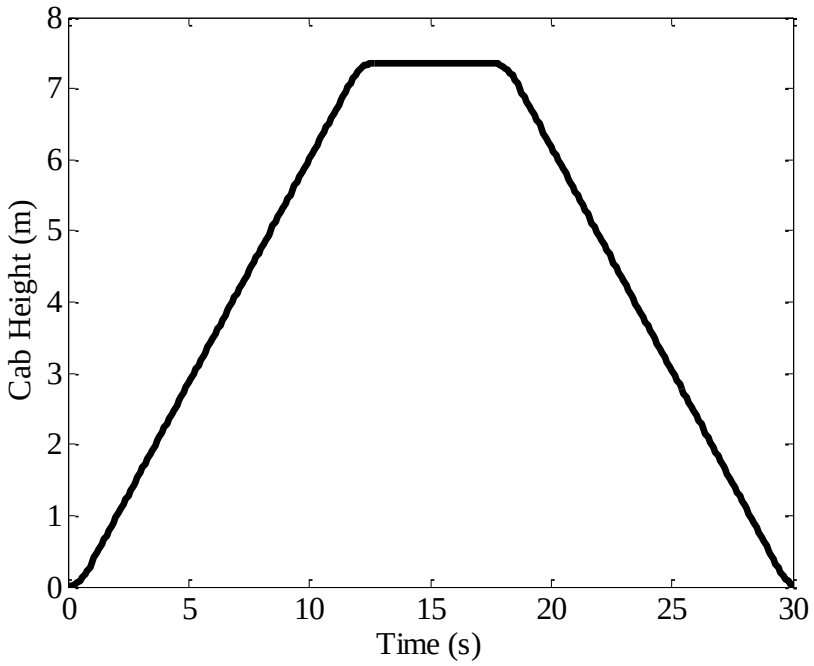

Figure 3.1: Pre-determined motion profile used for DP-informed Monte Carlo simulations.

To adequately determine a region of optimality, the Monte Carlo simulations consisted of using DP on 48 backward-looking simulations. Due to DP's high computational time associated with high discretization (discussed in the next section), the discretization of the discreet-time domain backward-looking simulations in this section was limited (~500 discretization points), in order to ensure timely computations. It should be noted that limiting the discretization of DP has the potential of resulting in a lack of convergence in the values of optimal energy consumption; however, the relative relationship of energy consumption between simulations is maintained. Maintaining the relative relationship of energy consumption still allows the Monte Carlo simulations to identify a region of optimality. The resulting data from the Monte Carlo simulations was able to identify an optimal region within the domain as shown in Figure 3.2.

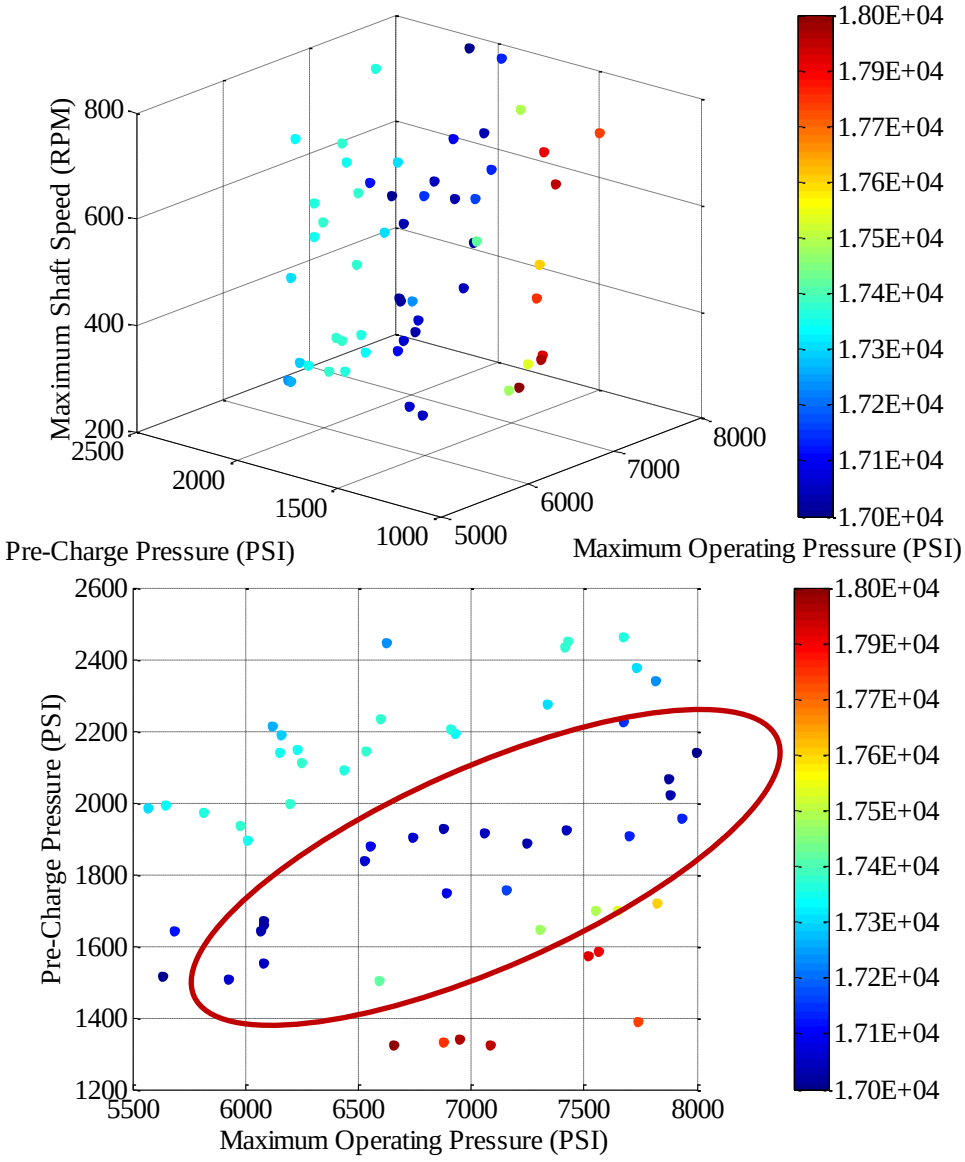

Figure 3.2: Region of Monte Carlo domain identified as optimal in 3D (top) and 2D (bottom) . Colorbar indicates DP-provided minimum value of energy usage (J).

The results demonstrate a region of optimal energy usage as circled in Figure 3.2 (bottom). The region presumably allows for several combinations of ω, P_{2max}, and P_{2pr}. However, the choices of P_{2max} and P_{2pr} define the size of Accumulator 2 as follows,

$$V_2 = \frac{0.4U_2}{\left(\left(\frac{P_{2max}}{P_{2pr}}\right)^{\frac{0.4}{1.4}} - 1\right)P_{2pr}} \tag{39}$$

This allows for the consideration of a smaller region than shown by Figure 3.2 since presumably, a smaller Accumulator 2 (smaller values of V_2) is preferable over a larger one. Larger accumulators are generally associated with higher costs. Figure 3.3 shows the $V_2 - P_{2max} - P_{2pr}$ relationship.

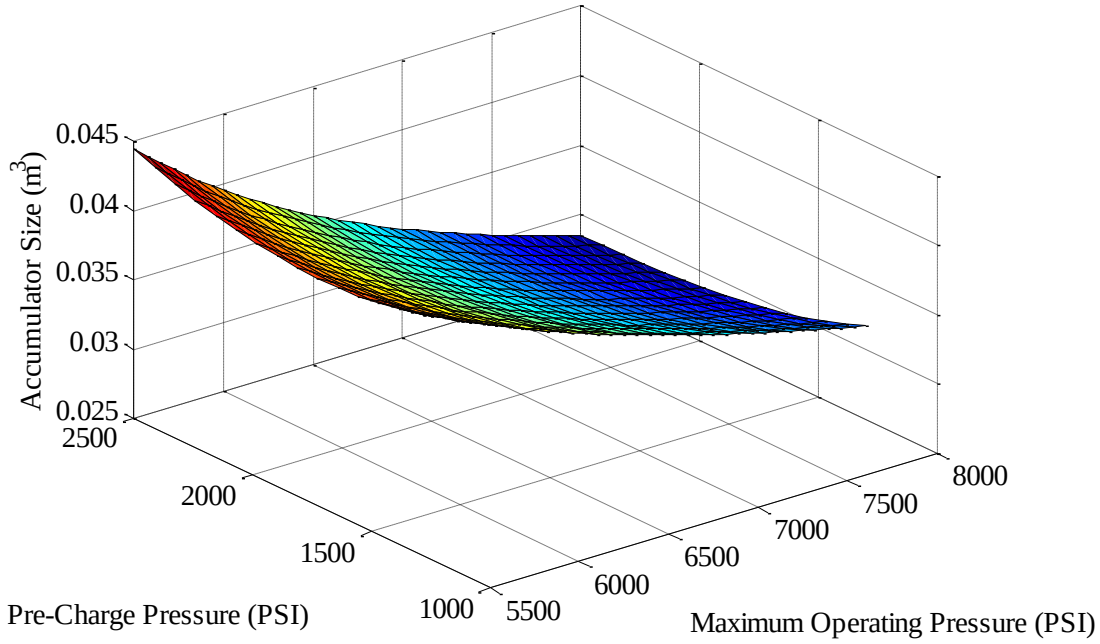

Figure 3.3: Volume of Accumulator 2 as a function of operating pressures.

Considering both Figure 3.2 and Figure 3.3 it is apparent than an optimal sizing of the system occurs at high values of P_{2max} (7000 – 8000 PSI) and values of P_{2pr} between 1800 – 2200 PSI; such that an efficient system is obtained while the resulting volume of Accumulator 2 is maintained relatively low. The DP-Informed Monte Carlo simulations can then conclude in the final values shown in Table 3.2.

Table 3.2: Final values for design degrees of freedom.

Parameter	Value
ω (RPM)	700
P_{2max} (PSI)	8000
P_{2pr} (PSI)	2000

3.2 Optimal Control of Novel Hydraulic Architecture: Elevator

Establishing a final sizing for the system using optimization methods tackles the gaps left by the heuristic approach to the sizing in Chapter 2 but does little to address the gaps left by a heuristic approach to control. Chapter 2 presented various efficiency considerations to develop a heuristic approach to controlling the architecture; however, as previously mentioned, the input in the SISO model of the system consists of a ratio of two independent values. This creates a non-uniqueness which allows for several supervisory control choices possible for a certain motion, each of which will yield varying system efficiencies. This gap left by the initial heuristic control approach warrants a more rigorous control approach based on optimization techniques such as DP.

3.2.1 Dynamic Programming

In the development of real-time controllers it is often unfeasible to achieve an optimal response from the system being controlled. Nevertheless, knowledge of the optimal controllers, despite their unattainability, can be an important skeleton upon which to build the implementable suboptimal controller. Such an optimal controller can be found using the deterministic optimization technique Dynamic Programming (DP) [35]. As

briefly stated in the last section, DP provides a globally optimal control path for a predetermined motion profile through the exploitation of Bellman's Principle of Optimality. The required knowledge of future inputs into the system (predetermined motion profile) most often renders the controller provided by DP non-causal; however, it is quite useful in developing a causal controller. Bellman's Principle of Optimality states that the optimality of a future control action will not be affected by the optimality of any past control action [36]. DP uses this principle to move backwards in time through a known motion profile of a system with identified states and control variables, and provides an optimal control path within constraints of the control space. In general, a DP algorithm is used on a class of discrete-time models in the following form,

$$x_{k+1} = F_k(x_k, u_k) \qquad k = [0, N-1] \tag{40}$$

where k denotes the index of discretized time, x_k the state variable, u_k the control variable, and F_k the function defining the state transition. The total cost of using the control strategy $\pi = \{\boldsymbol{u}_0, \boldsymbol{u}_1, \dots \boldsymbol{u}_{N-1}\}$ with the initial state x_o is,

$$J_{0,\pi}(x_0) = g_0(x_0) + g_N(x_N) + \phi_N(x_N) + \sum_{k=0}^{n-1} [h_k(x_k, u_k) + \phi_k(x_k, u_k)] \tag{41}$$

where $J_{0,\pi}(x_0)$ denotes a total cost, $g_{0/N}(x_{0/N})$ an initial/final cost, $\phi_k(x_k, u_k)$ a penalty function enforcing constraints on the state and control variables, and $h_k(x_k, u_k)$ an incremental cost of applying the control at time *k*. An optimal control policy is one that minimizes the total cost represented by $J_{0,\pi}(x_0)$.

3.2.2 Dynamic Programming Applied on Novel Hydraulic Architecture

Within the context of the proposed architecture and its application to a hydraulic elevator, DP is able to provide, for a prescribed schedule of height versus time, values in time for the PM displacements (the control space) which will result in changes in accumulator pressures (the state space) that move the actuator through the required motion profile such that energy input from the auxiliary EM (the cost) is minimized. In other words, the control path provided by DP is the time-history of control inputs (e.g., pump/motor displacements) which minimize the losses of the system.

The DP control problem of the system herein can be characterized as,

$$x = \left(P_1, P_2, P_{3,} h_{cab}\right) \tag{42}$$

$$u = (D_1, D_2, T_{EM}) \tag{43}$$

$$h_k = P_{out}(x, u) \tag{44}$$

The permissible values for both the control and state variables are,

$$P_{1pr} \leq P_1 \leq P_{1max} \tag{45}$$

$$P_{2pr} \leq P_2 \leq P_{2max} \tag{46}$$

$$P_{3pr} \leq P_3 \leq P_{3max} \tag{47}$$

$$0 \leq D_1 \leq D_{1max} \tag{48}$$

$$-D_{2max} \leq D_2 \leq D_{2max} \tag{49}$$

Violation of these values at any time step incurs a penalty cost, $\phi_k(\boldsymbol{x}_k, \boldsymbol{u}_k)$, of much larger value than the incremental cost thereby ensuring the resulting control path does not result in state or control constraints violations. It should be noted that the differing constraints for D_1 and D_2 ensure there is only one control input associated with a resulting state transition and cost. The 4-quadrant nature of the variable-displacement PM would allow for two different control inputs to be associated with one state transition and cost combination should they both be allowed their full range. This phenomenon may result in erratic behavior from DP in its choice for a control path due to the existence of two locally optimal choices for control inputs.

3.2.2.1 Reduction of Dynamic Programming Computation Time

The computation time of DP increases exponentially as the number of independent state and control variables increase. This is because DP sifts through all permissible values of each at each time step. It is therefore good practice to simplify the problem statement as much as possible before attempting to implement DP. For the particular case of the introduced architecture, certain constraints of operation allow for such a simplification. Specifically, since DP requires a predetermined schedule of height (h_{cab}) versus time, the values at each time step for h_{cab} are already known, consequently, because leakage losses in the system manifest only as a loss in pressure, and not a physical loss of fluid, P_1 and h_{cab} are related by flow continuity,

$$P_1 = \left(P_{1pr} + P_a\right)\left(1 - \frac{V_{1fluid} - Ah_{cab}}{V_1}\right)^{1.4} - P_a \tag{50}$$

Similarly, the pressures P_2 and P_3 can also be related using flow continuity,

$$P_3 = \left(P_{3pr} + P_a\right)\left(1 - \frac{V_{2fluid} - v_{2fluid}}{V_3}\right)^{1.4} - P_a \tag{51}$$

Where v_{2fluid} is the current volume of fluid in Accumulator 2 as a function of P_2 given by,

$$v_{2fluid} = V_2\left(1 - \frac{P_{2pr} + P_a}{P_2 + P_a}\right)^{\frac{1}{1.4}} \tag{52}$$

These constraints reduce the independent states to simply $x = (P_2)$. A similar simplification can be conceived with respect to the control variables by virtue of the predetermined height profile. The calculated incremental cost P_{out} is related to T_{EM} by ω, which is in turn defined by h_{cab} and D_1 at each time step,

$$T_{EM_k} = \frac{P_{out_k}}{\omega_k} \tag{53}$$

$$\omega_k = \frac{Av_k}{D_1} \tag{54}$$

$$v_k = \frac{h_{k+1} - h_k}{\Delta t} \tag{55}$$

where Δt is the time increment between time steps. This relationship simplifies our control variables to $u = (D_1, D_2)$.

Despite the reduction of the control variables and the state variables in the application of DP to this architecture, highly discretized runs of DP still require an exceptionally large computational time. To remedy this, parallelization of the DP code was performed, possible by virtue of it being a backward-looking simulation. The parallelization sought to execute computationally demanding parts of the code simultaneously and then piece

together the resulting stored data to produce final control and state paths. This was done by running multiple instances of Matlab simultaneously on a 64-core machine and suppressing the desktop windows of Matlab using linux source code. The code was able to compute the relevant values associated with each value of P_2 at each time step (u, h_k) for multiple values of P_2 simultaneously; such that if, for example, the non-parallelized code of DP would iterate in order through P_{2a}, then P_{2b}, and then P_{2c}, the parallelized code was able to compute the relevant values for P_{2a}, P_{2b}, and P_{2c} simultaneously. The resulting code was able to perform a satisfactorily discretized run of DP (2000 state and control discretization points) with an acceptable computational time (24 hours) at the expense of requiring more storage space.

3.2.2.2 Optimal Control of Architecture Using Dynamic Programming

DP was applied to the hydraulic architecture under three different load cycles so as to capture the varying operation encountered in an elevator application. All load cycles were contemplated undergoing the same motion profile, shown below (Figure 3.4).

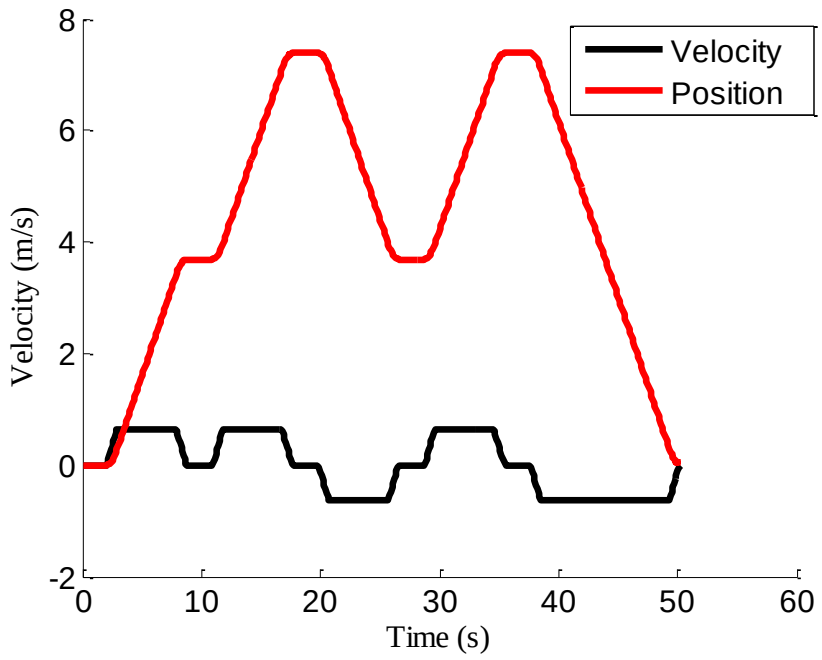

Figure 3.4: Motion profile used for Dynamic Programming

The cab travels from the 1st floor up to the 2nd floor, then further up to the 3rd floor, back down to the 2nd floor, up to the 3rd floor again, and finally back down to the 1st floor. In the first of these load cycles, heretofore Load Cycle 1, a situation in which the elevator would descend with more people than it ascends was contemplated (presumably the case in the evening, for commercial applications). In this case the elevator is gaining more energy than it loses as it ascends with an empty cab (1100 kg) and descends with a full cab (2070 kg). The resulting control path suggested by DP is pictured in (Figure 3.5). The corresponding state path can be seen in Figure C1 in Appendix C.

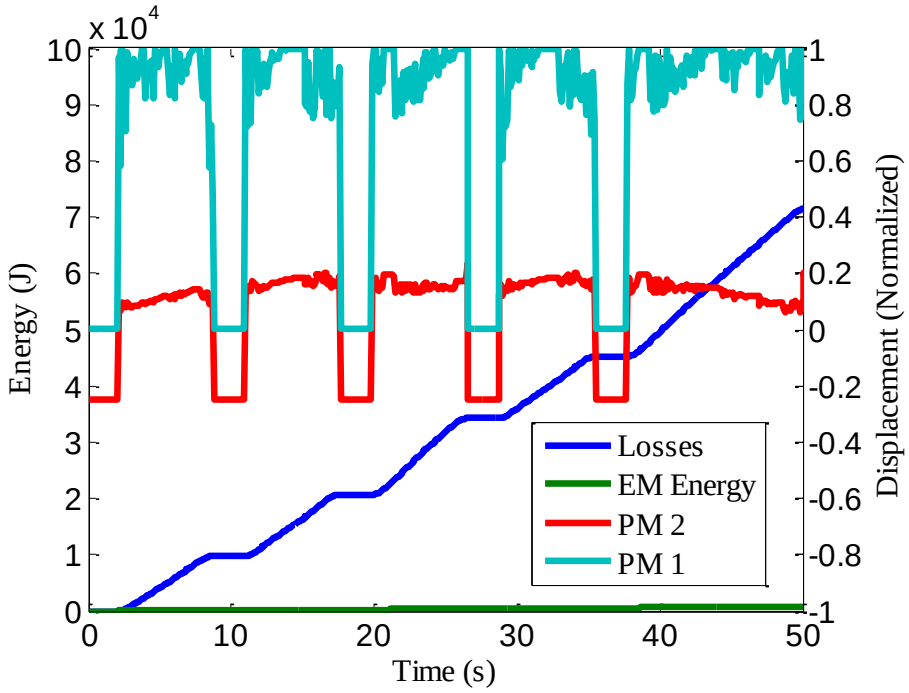

Figure 3.5: Control path suggested by Dynamic Programming: Load Cycle 1

It should be noted that in this load cycle the EM can be seen to have minimal activity throughout. This is expected as the losses of the system are being overcome by the net energy gain resulting from ascending with a smaller load than that of descent.

In the second of these load cycles, heretofore Load Cycle 2, the elevator descends with an empty cab and ascends with a full cab, resulting in a net energy loss. The resulting control path suggested by DP is picture in Figure 3.6. The corresponding state path can be seen in Figure C2 in Appendix C.

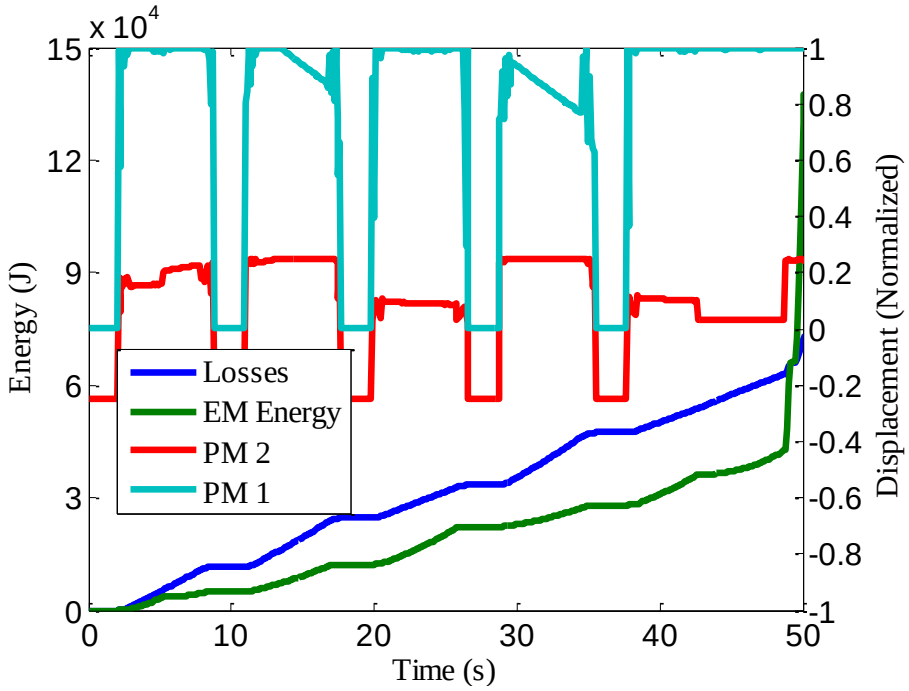

Figure 3.6: Control path suggested by Dynamic Programming: Load Cycle 2

It should again be noted that the suggested control implies more energy is input into the system than what is lost. The EM having to compensate from both, the energy loss of the system throughout motion as well as the energy loss due to the loss of potential energy upon descent, explains this.

In the third and final of the load cycles, heretofore Load Cycle 3, the elevator descends and ascends with a constant load (full cab). The resulting control path suggested by DP is pictured in Figure 3.7. The corresponding state path can be seen in Figure C3 in Appendix C.

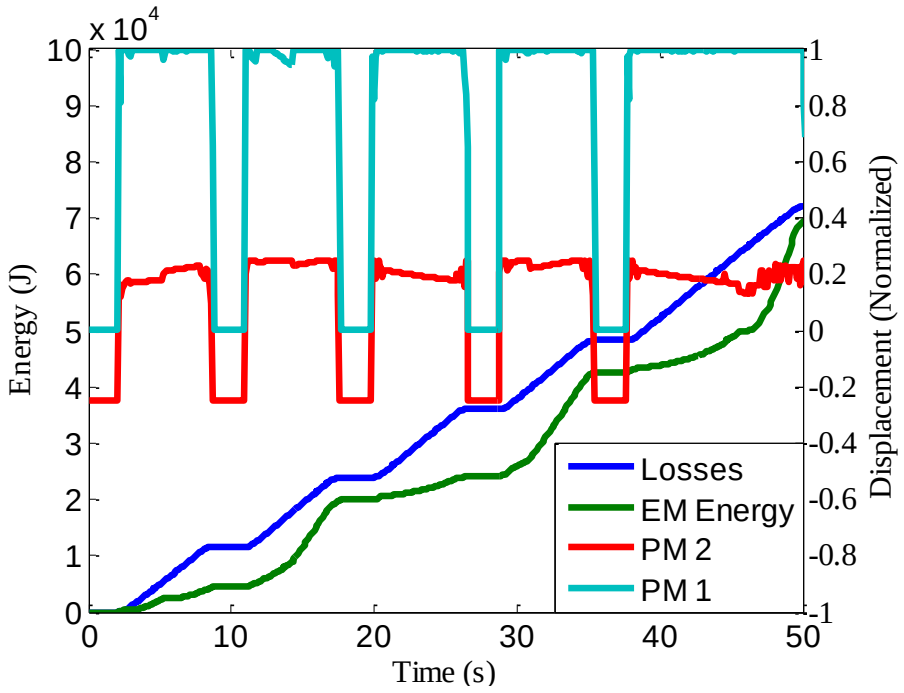

Figure 3.7: Control path suggested by Dynamic Programming: Load Cycle 3

Predictably, in this case, we see the EM input exactly the amount of energy lost, save for a small gap due to the discretized nature of the simulation.

The objective of the DP studies was to extract certain characteristic of optimal control of the architecture across its operation. These characteristic would then be used in a real-time forward-looking simulation. As is apparent from Figures 3.5-3.7, the optimal control path of the system varies considerably depending on the load cycle. Nevertheless, certain characteristics of optimal control can be extracted from the figures. Specifically, all figures show an optimal control path which opts to maximize or nearly maximize the displacement of PM_1. Additionally, the two load cycles with an appreciable activity from the EM show a tendency for the EM to meet the final constraint of refilling Accumulator 2 by operating intensively during the end of motion. This is not much different from the heuristic control rules developed in Chapter 2; which in a sense are now validated not only by efficiency considerations but by DP.

3.3 DP-Informed Rule-Based Control of Novel Hydraulic Architecture: Elevator

3.3.1 Development and Implementation of Rule-Based Controller

Despite the similarity between the heuristic control rules and those gleaned from DP in the last section, the final DP-informed rule-based controller contains some changes. Mainly, the value for the displacement of PM_1 is set to its maximum, per the suggestion from DP. Additionally, EM operation now responds to information given by the position of the actuator instead of the velocity, specifically, desired and current height (floor, in the case of the elevator) information is used to determine if the load is descending. Similar to the heuristic control in Chapter 2, upon descent, the EM is instructed to operate such that the value of P_2 upon reaching the desired height is one that will be able to lift a full cab up to the highest floor; this required value for P_2 is defined by the desired height. In the scenario where more load descends than ascends, as is the case of Load Cycle 1, the EM will discontinue input if the required value for P_2 is reached before the load reaches the desired height. In summary, the controller uses state information (current floor, desired floor, and Accumulator 2 Pressure) to operate the architecture. Required Accumulator 2 pressure, P_2, at a given desired height, $h_{desired}$, is given by the following relationship,

$$P_2 = \left(\frac{\beta[0.4mg(h_{max} - h_{desired})]}{V_2} + P_{2pr} \right)^{\frac{1.4}{0.4}} \tag{56}$$

Where β is a multiplier greater than 1 that results in higher pressure values than theoretically desired to account for inefficiencies of the system during ascent. For this particular application β = 1.1 is sufficient.

Figure 3.8 shows the architecture with the corresponding rule-based controller and its outputs/inputs. The corresponding Simulink diagram can be found in Figure C4 in Appendix C.

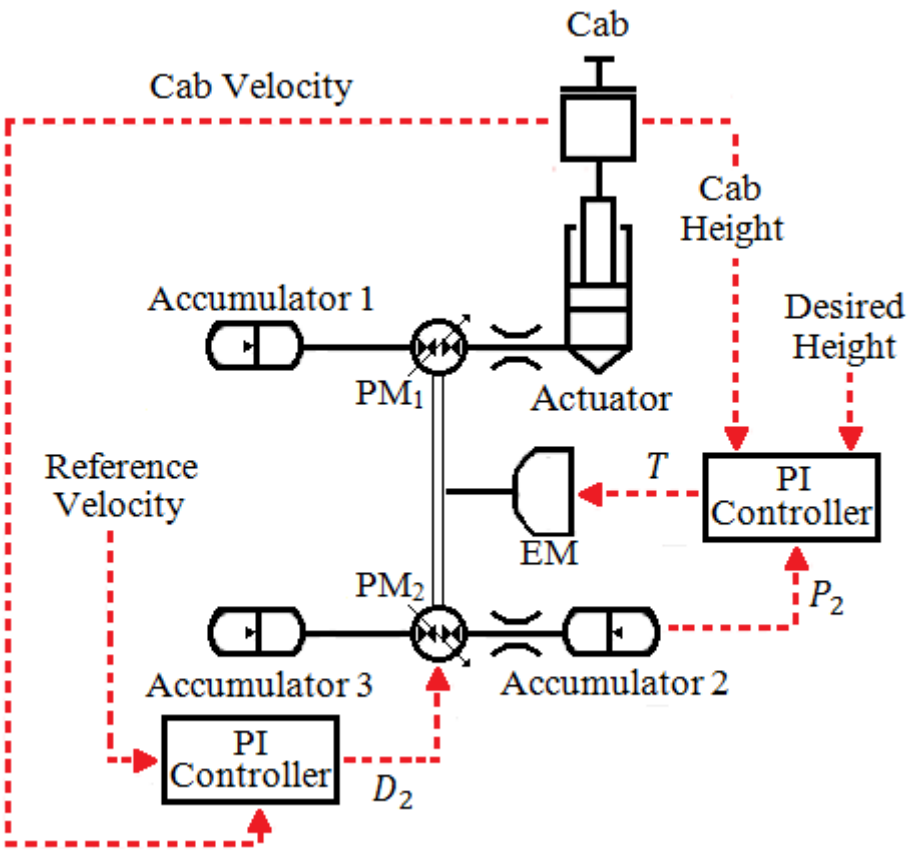

Figure 3.8: Hydraulic architecture with accompanying rule-based controllers

Figure 3.9 shows the results from implementing this rule-based controller on the same motion profile as that used in Section 3.2.2.2, using Load Cycle 3. The same results using Load Cycle 1 and 2 are seen in Figure C5 and Figure C6 respectively, in Appendix C.

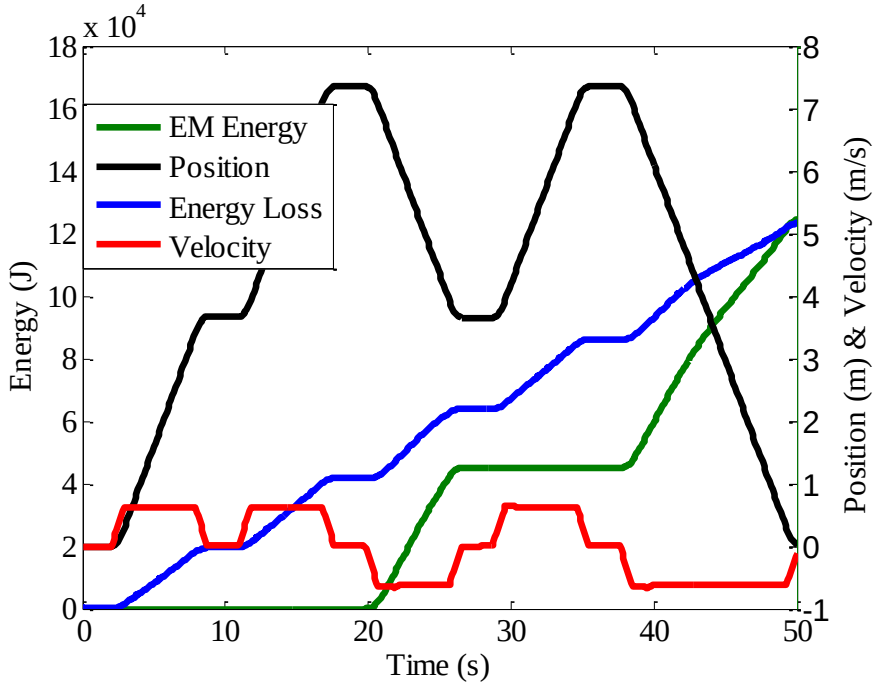

Figure 3.9: Architecture performance using DP-informed rule-based controller: Load Cycle 3

3.3.2 Comparison of Rule-Based Control with Dynamic Programming

Comparing the performance of the rule-based controller with that of DP is an useful way to measure the degree of optimality of the developed controller. This comparison, for all three load cycles is shown in Figure 3.10.

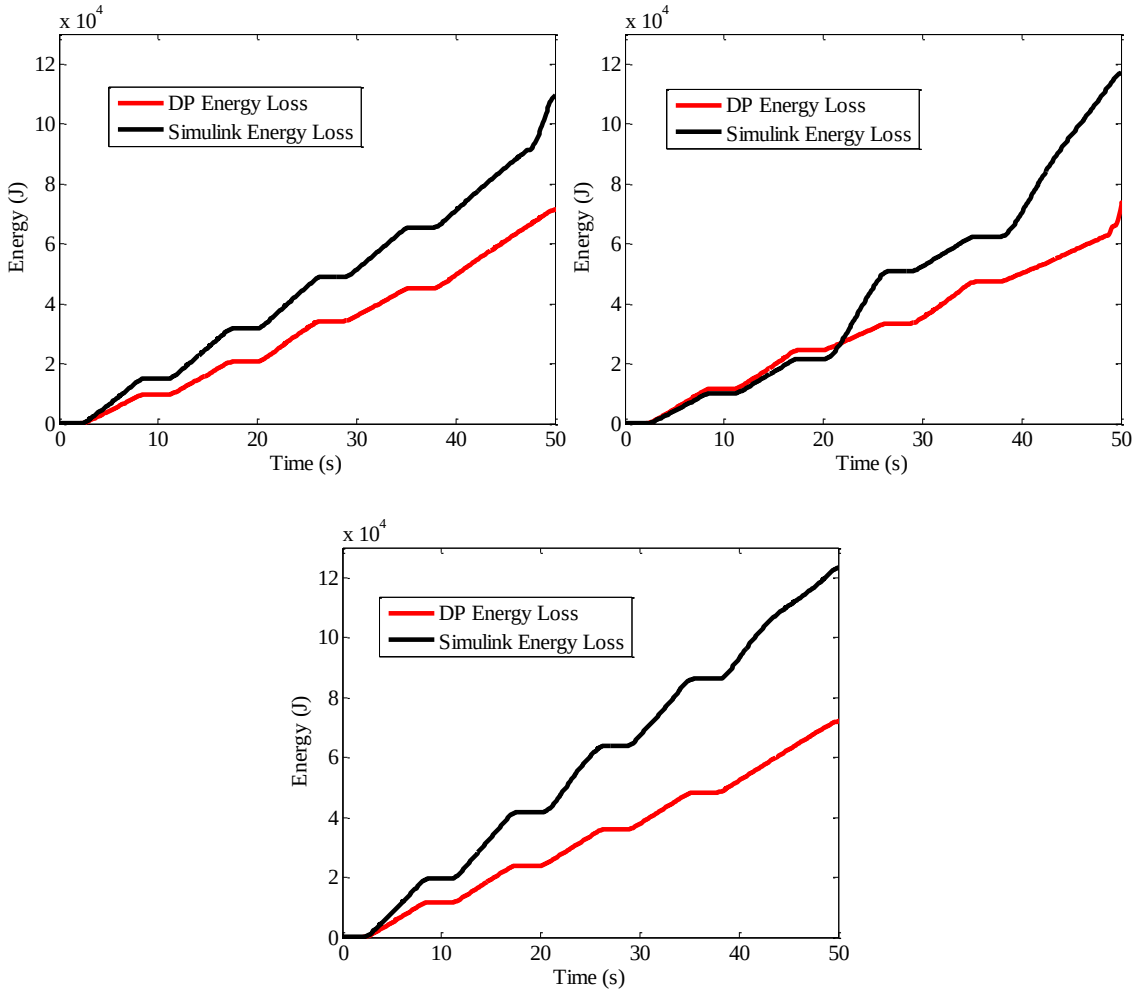

Figure 3.10: Comparison of energy consumption between rule-based controller and Dynamic Programming for Load Cycle 1 (top left), Load Cycle 2 (top right), and Load Cycle 3 (Bottom)

From the figure, the rule-based controller can clearly be seen to be suboptimal as it induces levels of energy loss throughout motion higher than those calculated by DP. The level of optimality of the controller can be calculated by averaging that of all three load cycles, with the understanding that many other load cycles are possible which may exhibit small changes in the level of optimality. The calculation for the level of optimality is simply,

$$\% \, Optimal = \frac{E_{Loss_{DP}}}{E_{Loss_{Simulink}}} * 100\% \quad (57)$$

By averaging the result of (57) for all three load cases in Figure 3.10, the rule-based controller is determined to be 62% optimal.

3.3.3 Comparison of DP-Informed Architecture with Initial Heuristic Architecture

Achieving high levels of optimality from the architecture after having optimized both the sizing and control of the system is desirable, nevertheless, the merits of the optimization process performed on the architecture are best seen when the DP-Informed system is compared to its original heuristic counterpart. This section demonstrates the improvement achieved through the optimization process by comparing the energy loss of the DP-Informed system versus that of the heuristic system. Figure 3.11 shows such a comparison for the motion profile in Section 3.2.2.2 and Load Cycle 3.

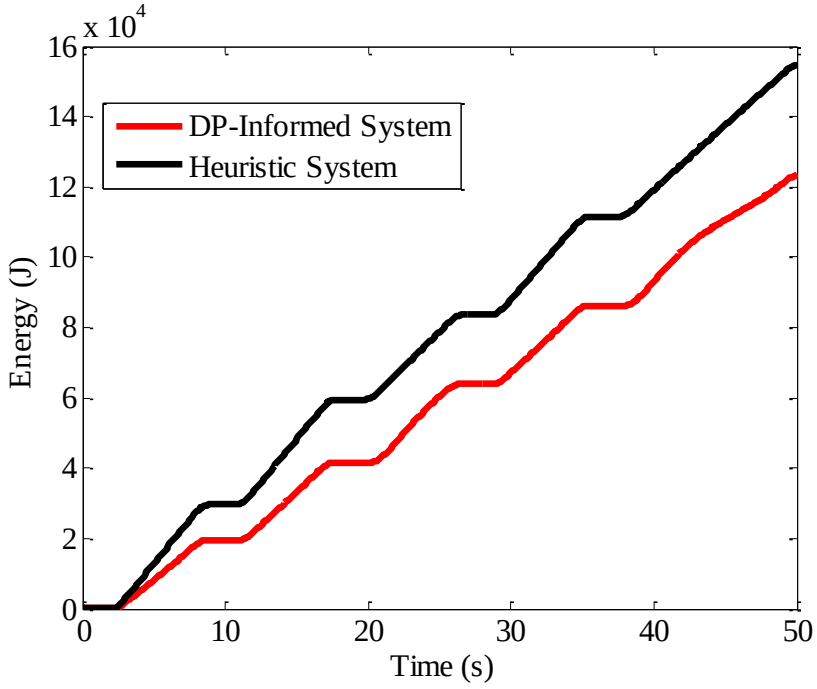

Figure 3.11: Comparison of energy usage between DP-informed rule-based system and heuristic system.

The figure shows that the DP-Informed system achieves an efficiency improvement of 21% compared to the heuristic system.

3.4 Optimization process on the forklift

Much of this thesis has been dedicated to the novel hydraulic architecture as applied to the hydraulic elevator; this is due to the significant benefits the industry would experience from improved efficiency. Nevertheless, in addition to the hydraulic elevator, Chapter 1 identified the hydraulic forklift as another potential application for the introduced hydraulic architecture. In summary, the conventional fork lift involves a hydraulic circuit similar to that of the conventional elevator wherein the main speed control component is the throttling of fluid through a valve. The high inefficiencies have prompted similar attempts (as those made on the hydraulic elevator) at recovering electrical energy from its motion. Consequently, this section employs the optimization

process discussed in Sections 3.1-3.3 on the hydraulic forklift to demonstrate a similar resulting level of optimality achieved; thereby suggesting the introduced architecture as an advantageous alternative to current hydraulic forklift architectures.

3.4.1 Optimal sizing of Novel Hydraulic Architecture: Forklift

3.4.1.1 Preliminary Sizing

The primary difference between applications of hydraulic lifting is often the load cycle. Consequently, the sizing procedure for the forklift is very similar to that of the elevator, as much of it is defined by the hydraulic circuit rather than the load cycle. However, the load cycle does define the size of Accumulator 2 and different motion parameters also affect certain components. For this thesis, the work from Minav is used to define the load cycle and motion parameters of the hydraulic forklift [21, 37]. Specifically, the motion parameters and some of the load cycle parameters used can be seen in Table 3.3.

Table 3.3: Motion and load parameters for sizing procedure: Forklift

Parameter	Value
$a_{max}\left(\frac{m}{s^2}\right)$	0.30
$v_{max}\left(\frac{m}{s}\right)$	0.44
$m_{max}\,(kg)$	998
$m_{min}\,(kg)$	250
$h_{max}\,(m)$	3.4

Furthermore, the load cycle of the forklift presented by Minav, and used herein, contemplates a simple lifting-lowering cycle tested at different payloads such that 5

consecutive payloads are lifted to maximum height or lowered from maximum height. Accumulator 2 will therefore need to store, at most, the energy equivalent of 5 full payloads being lowered from maximum height. Consequently, the expression for U_2 used in the sizing procedure of section 3.2.1 can now be expressed by,

$$U_2 = 5m_{max}gh_{max} \tag{58}$$

It is important to note that it is difficult to generalize the load cycle of a forklift (unlike that of an elevator) and large deviations from the load cycle assumed can significantly affect the resulting size of Accumulator 2. For purposes of demonstrating the optimization procedure on the proposed architecture, the assumed load cycle was deemed sufficient.

3.4.1.2 DP-Informed Monte Carlo Sizing

The Monte Carlo Simulations performed in section 3.1.2 were repeated here in the context of the hydraulic forklift. Figure 3.12 displays the results and corresponding optimal sizing region.

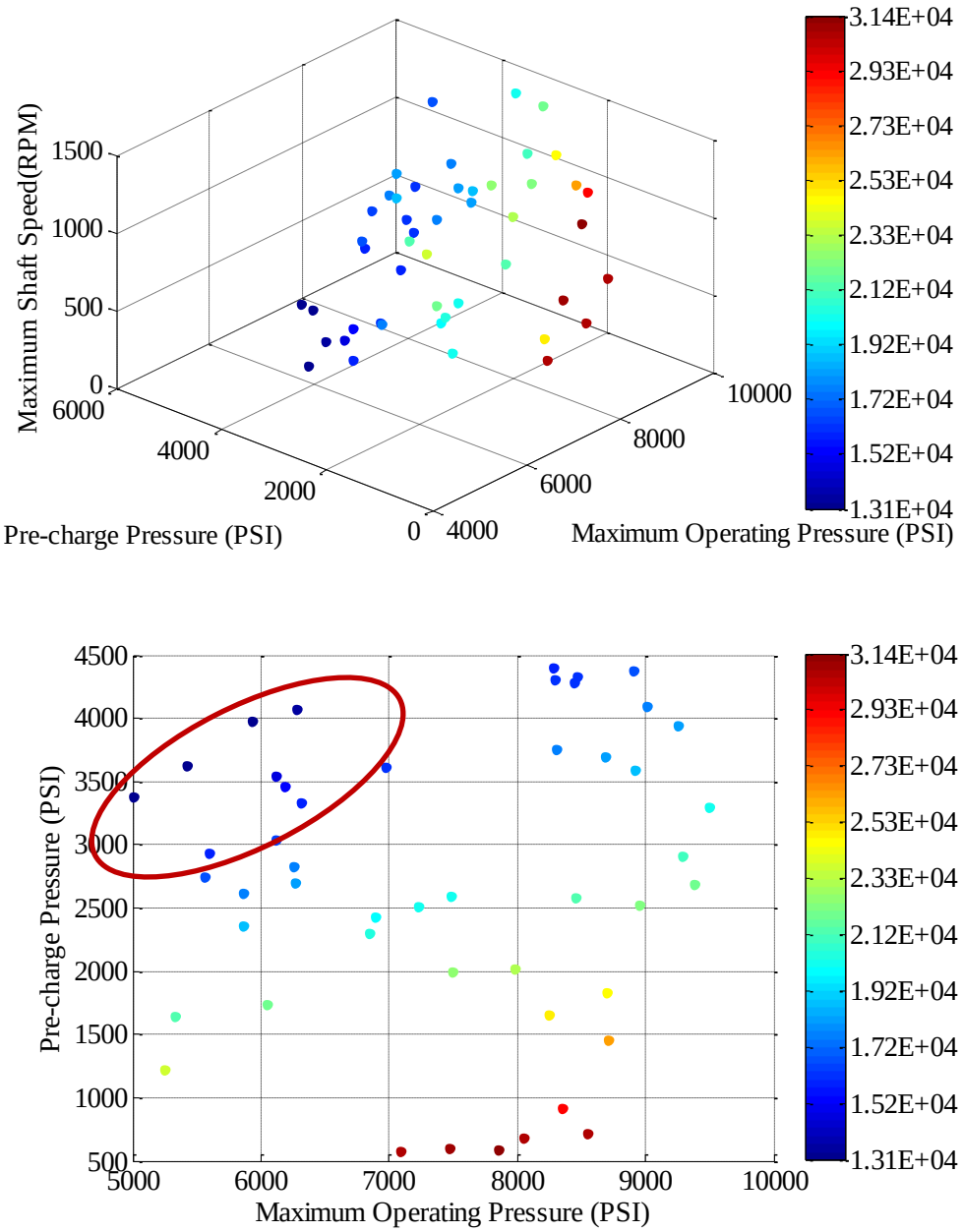

Figure 3.12: Region of Monte Carlo domain identified as optimal in 3D (top) and 2D (bottom): Forklift. Colorbar indicates DP-provided minimum value of energy usage (J).

Using the same volume considerations for a gas-charged accumulator, the final sizing values for the DDOF are shown in Table 3.4

Table 3.4: Final values for design degrees of freedom: Forklift

Parameter	Value
ω (RPM)	500
P_{2max} (PSI)	6000
P_{2pr} (PSI)	3500

3.4.2 Optimal control of Novel Hydraulic Architecture: Forklift

The DP problem statement on the hydraulic architecture remains unchanged between the hydraulic elevator and hydraulic forklift; that is to say, the same state and control variables are maintained. Nevertheless, a different motion profile is used, shown by Figure 3.13.

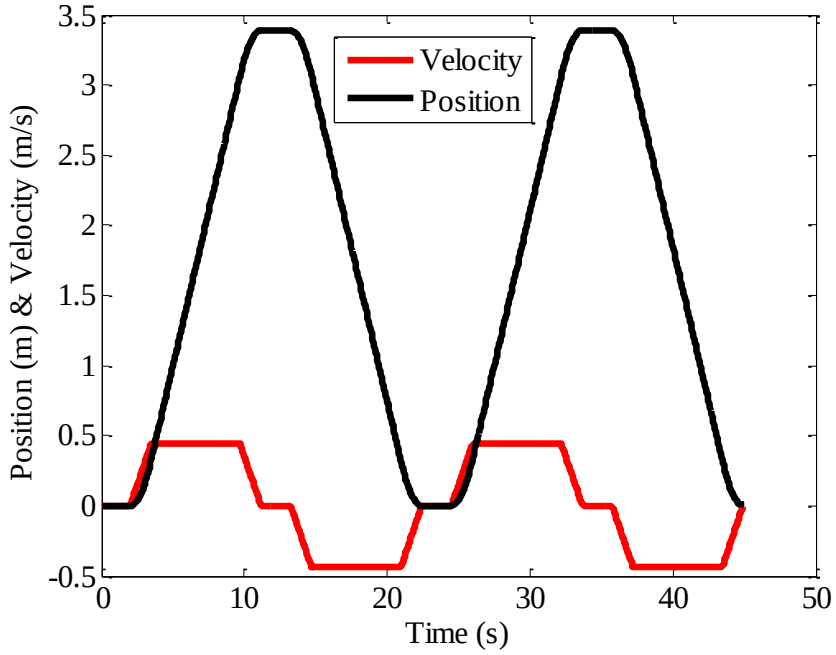

Figure 3.13: Motion profile used for Dynamic Programming: Forklift

The figure shows the fork moving up to maximum height and down to zero height, twice. One load cycle is used - a full load being lifted and an empty fork descending. The resulting control and state paths suggested by DP are shown in Figure 3.14.

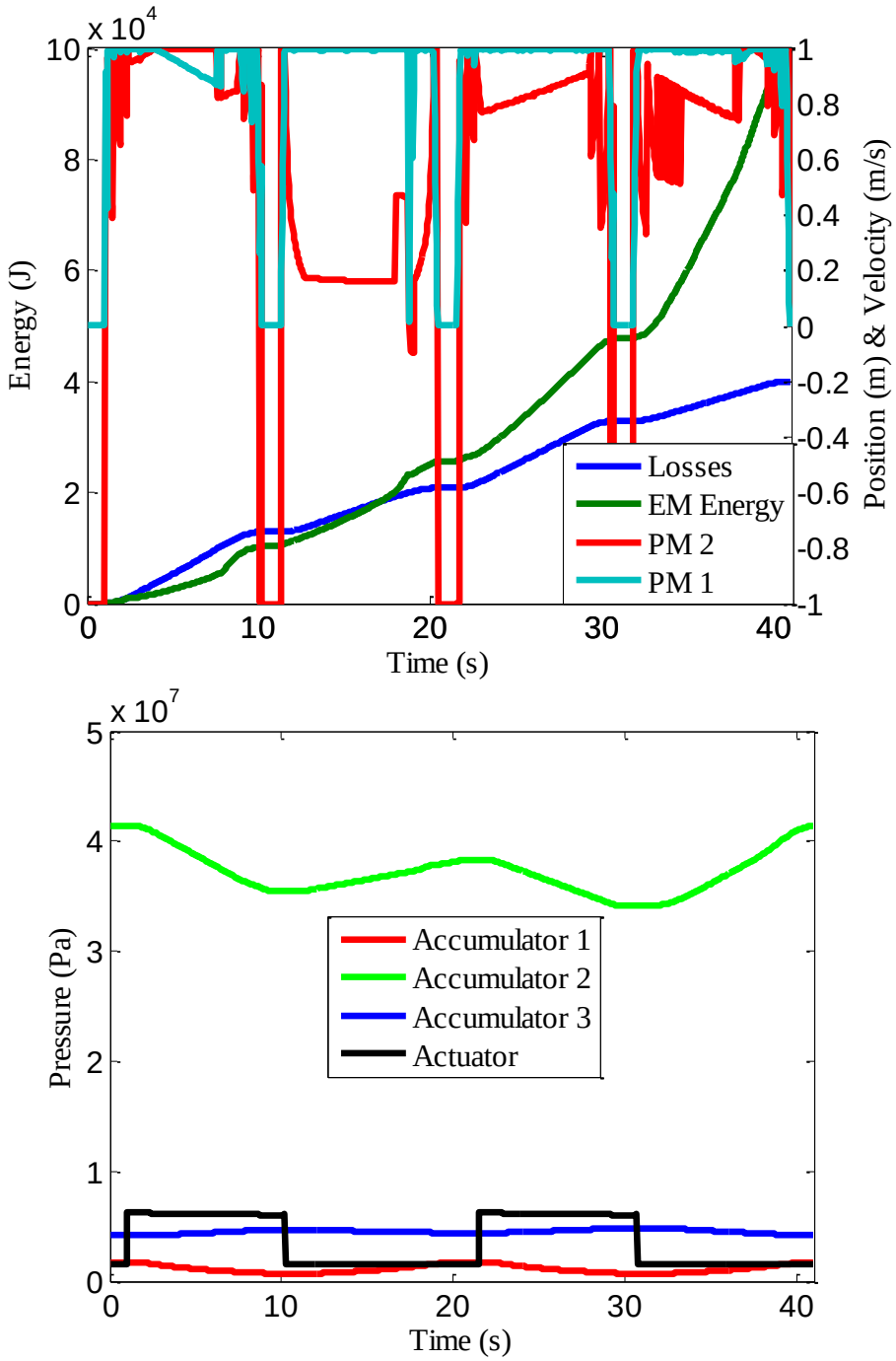

Figure 3.14 Control (Top) and state (Bottom) paths suggested by Dynamic Programming: Forklift

The characteristics of optimal control extracted from DP on the hydraulic forklift are quite similar to those extracted from DP on the hydraulic elevator. Displacement of PM_1 is maximized while the EM opts to fully recharge Accumulator 2 on descent. This similarity is presumably because efficient control is architecture specific rather than application specific. Although, the similarity between Load Cycle 2 and the load cycle used for the forklift may also explain this.

3.4.3 DP-Informed Rule-Based Control of Novel Hydraulic Architecture; Forklift

Despite the similarity between the characteristics of optimal control between the hydraulic forklift and the hydraulic elevator, the rule-based, implementable controller contains some changes which respond to the nature of the application. In particular, the forklift has no notion of "desired floor" and as such cannot use that information to decide if it is descending. Instead, the rule-based controller uses the load velocity to determine if the load is descending. Therefore EM operation now responds to information given by the velocity of the actuator instead of the position. Nonetheless, similar to the rule-based controller for the elevator, upon descent, the EM is instructed to operate such that the value of P_2 upon reaching the floor is one that will be able to lift a full cab up to the highest height. In the scenario where more load descends than ascends, the EM will discontinue input if the required value for P_2 is reached before the load reaches the floor. In summary, the controller uses state velocity and pressure information to operate the architecture. Required Accumulator 2 pressure, P_2, at the floor is given by the following relationship,

$$P_2 = \left(\frac{\beta[0.4mg(h_{\max_{\mathrm{FL}}})]}{V_2} + P_{2pr} \right)^{\frac{1.4}{0.4}} \tag{59}$$

Where β is a multiplier greater than 1 that results in higher pressure values than theoretically desired to account for inefficiencies of the system during ascent. For this particular application β = 1.05 is sufficient.

Figure 3.15 shows the architecture with the corresponding rule-based controller and its outputs/inputs.

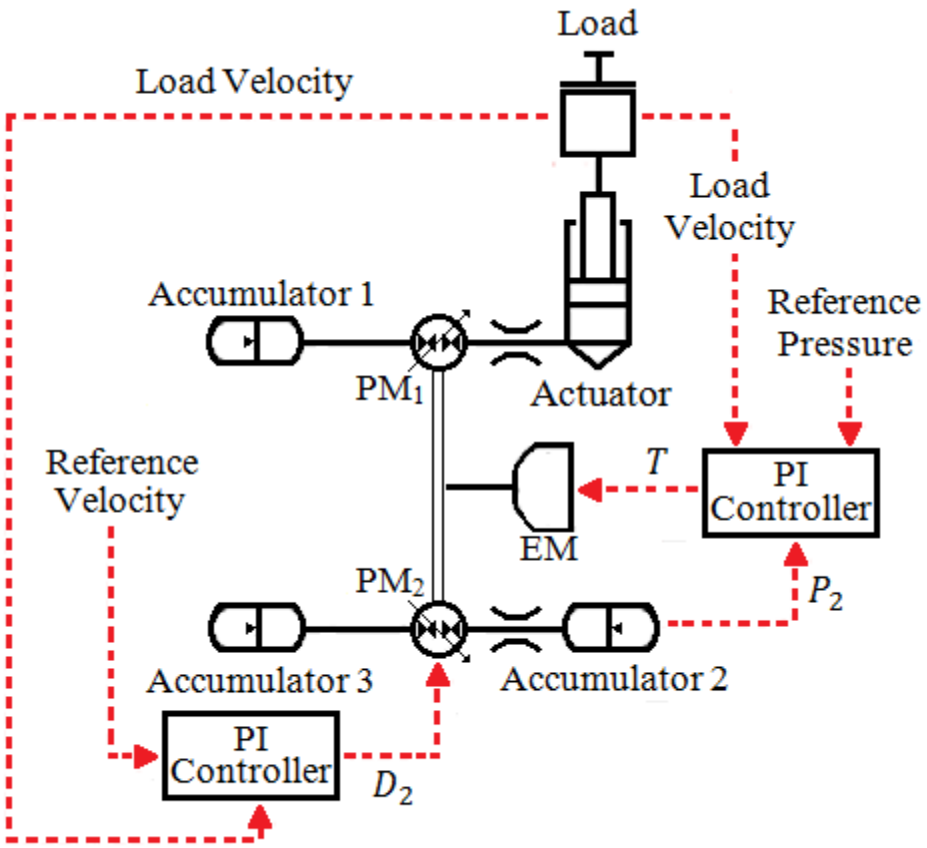

Figure 3.15: Hydraulic architecture with accompanying rule-based controllers: Forklift

The resulting operation from using the rule-based controller can be seen in Figure 3.16

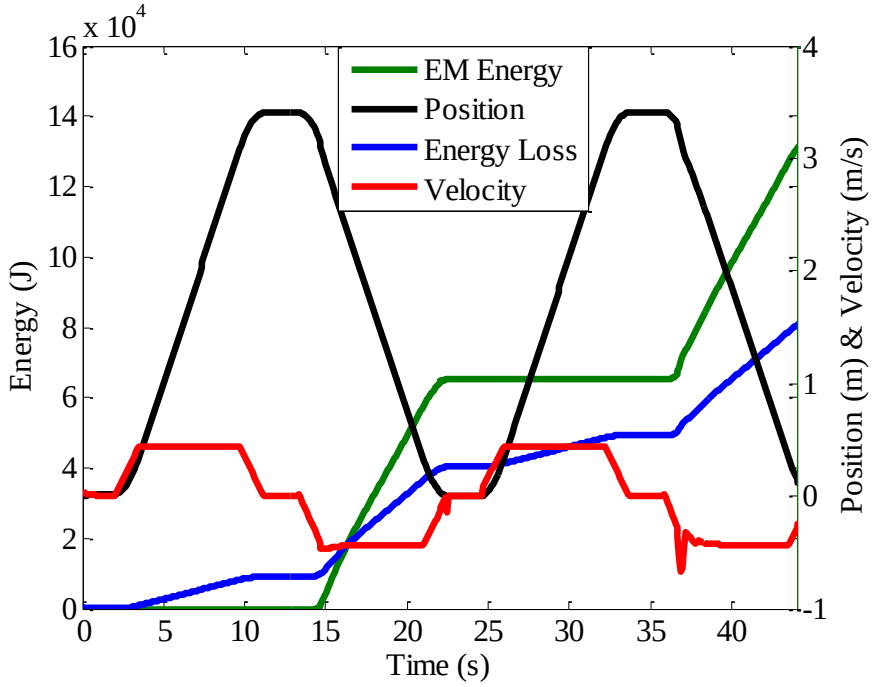

Figure 3.16: Architecture performance using DP-informed rule-based controller: Forklift

3.4.3.1 Comparison of Rule-Based Control with Dynamic Programming; Forklift

Much like that done for the hydraulic elevator, the optimization process can be assessed by comparing the performance of the rule-based control strategy to that of DP. Figure 3.17 shows this comparison.

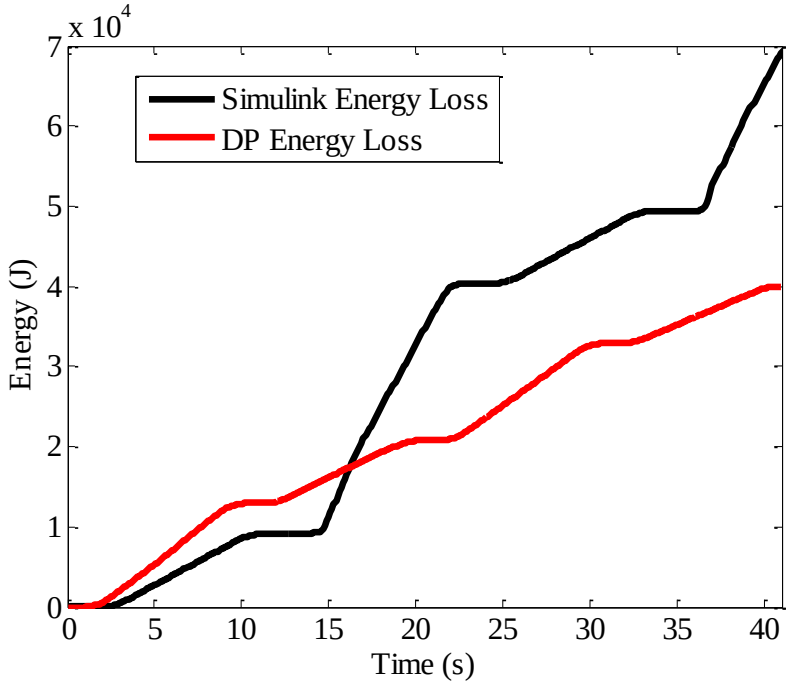

Figure 3.17: Comparison of energy consumption between rule-based controller and Dynamic Programming

From the figure, the rule-based controller can again be seen to be suboptimal, reaching an optimality level of 51%; a result similar to, albeit a bit lower than the hydraulic elevator.

3.5 Summary

Chapter 3 of this thesis ventured beyond the heuristic considerations for control and sizing of the introduced hydraulic architecture in the context of a hydraulic elevator. A preliminary sizing procedure was presented and a set of 3 DDOF identified; their existence warranted efforts at arriving at optimal values for them. DP-informed Monte Carlo simulations were performed to determine optimal values for the DDOF. Monte Carlo simulations yielded a region of optimality within the space formed by the DDOF. The final values for the DDOF were chosen according to the region identified by the Monte Carlo simulations. Characteristics of optimal control were determined through the

employment of DP on a backward-looking simulation. DP was applied on the architecture undergoing three different load cycles. The results identified two main characteristics of optimal architecture control: 1) the maximization of D_1 and 2) the use of the EM upon descent. A rule-based controller was developed on a forward-looking simulation using the characteristics of optimal control determined. Energy usage from the forward-looking simulation was compared to that of DP and found to be 62% optimal. Energy usage from the DP-informed architecture was then compared to that of the heuristically developed architecture in Chapter 2 and found to be 21% less; these results validated the optimization process undertaken. DP optimization process was used on a second application: the hydraulic forklift. Sizing, optimal control, and rule-base control were all performed in the context of the hydraulic forklift. Energy usage from the resulting forward-looking simulation was compared to that of DP and found to be 51% optimal.

CHAPTER 4

CONCLUSION AND FUTURE WORK

This thesis introduced and developed a novel hydraulic actuation architecture. Chapter 2 explored the architecture and its advantages over contemporary technology, in the context of the hydraulic elevator. Specifically, the introduced architecture achieved controlled actuation without relying on the use of throttling; the merits of the introduced architecture were identified against a traditional throttle-based architecture and further validated against a state-of-the-art electrohydraulic architecture. Results implied a strong advantage from the introduced architecture over technologies to which it was compared.

Chapter 3 of this thesis employed optimization techniques such as Dynamic Programming (DP) and Monte Carlo simulations to inform and improve the system in its control and its sizing, again in the context of the hydraulic elevator. The procedure moved beyond heuristic development of the architecture. DP-Informed Monte Carlo simulations were performed to achieve an optimal sizing of the system. Subsequently, DP-Informed rule-based control of the system was developed and implemented in a forward-looking simulation. The resulting system achieved adequate optimality and compared favorably to the heuristically developed version of Chapter 2. Lastly, the optimization procedure was employed in the context of the hydraulic forklift wherein it was shown to achieve moderate optimality. The optimality achieved was similar to that of the elevator; this alongside the similarities in current throttling technologies used for both suggests the introduced architecture as an advantageous alternative to current hydraulic forklift architectures as well.

4.1 Virtues of Novel Hydraulic Architecture

The novel hydraulic architecture introduced in this thesis underwent extensive research in order to identify its merits. Comparison with other hydraulic actuation architectures found the architecture to be of higher efficiency in relation. Specifically, for an elevator application, the introduced architecture displayed up to a 13% increase in efficiency of actuation and 23% reduction in daily energy consumption as compared a state-of-the-art electrohydraulic architecture. Additionally, the introduced architecture promised upwards of 75% reduction in daily energy consumption as compared to a conventional throttling architecture. Further investigation into the architecture identified presumably larger gains in efficiency. An optimization process involving optimal sizing and control of the architecture yielded a 62% energy optimal system and a 21% improvement in energy expenditure over initial heuristic implementation of the architecture. When applied in the context of a hydraulic forklift, the optimization process achieved a 51% optimal system.

4.2 Prototype of Novel Hydraulic Architecture

The results presented throughout this thesis establish the novel hydraulic architecture as an attractive technology for hydraulic actuation that may overcome the efficiency problems plaguing the industry today. Nevertheless, computational research, while vital in properly assessing a problem, fails to capture many issues that often arise while in practice. Future work on this architecture should focus on the development of a prototype of the novel hydraulic architecture which can incorporate all the nuances associated with practical implementation; therefore maintaining the horizon set on commercialization of the architecture.

APPENDIX A

SUPPLEMENTARY MATERIAL TO CHAPTER 1

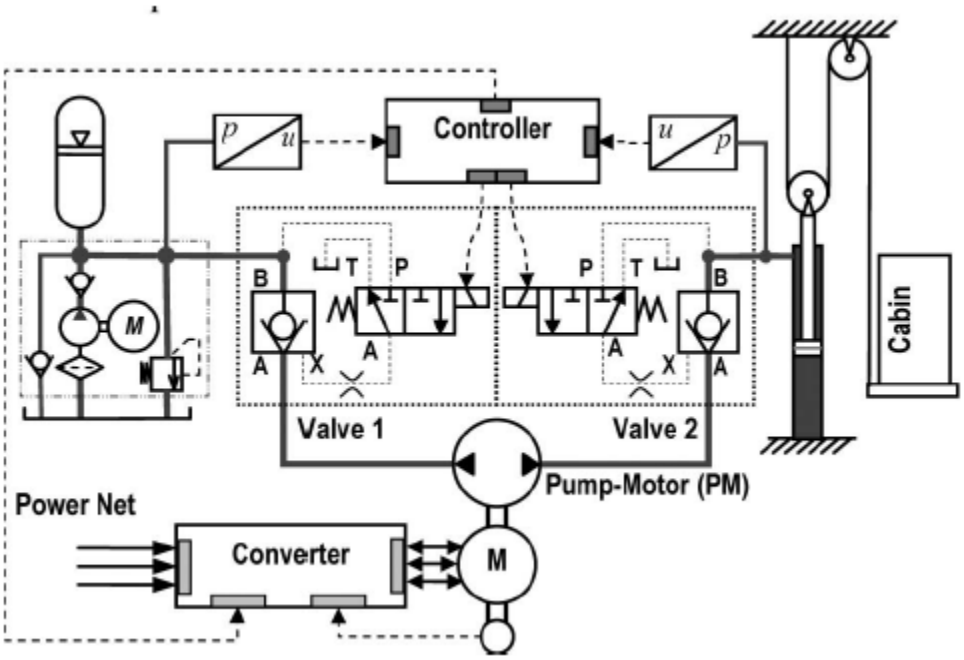

Figure A1: Electrohydraulic system patented by Bucher Hydraulics. Reproduced from [19]

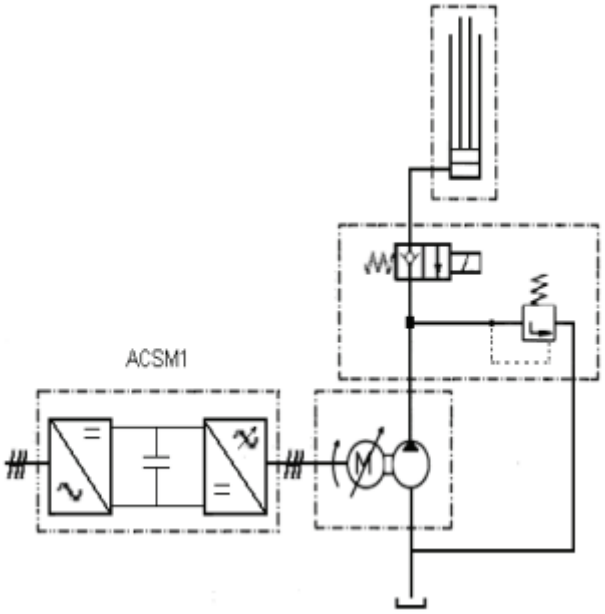

Figure A2: Schematic of test setup for hydraulic forklift. Reproduced from [21]

APPENDIX B

SUPLEMENTARY MATERIAL TO CHAPTER 2

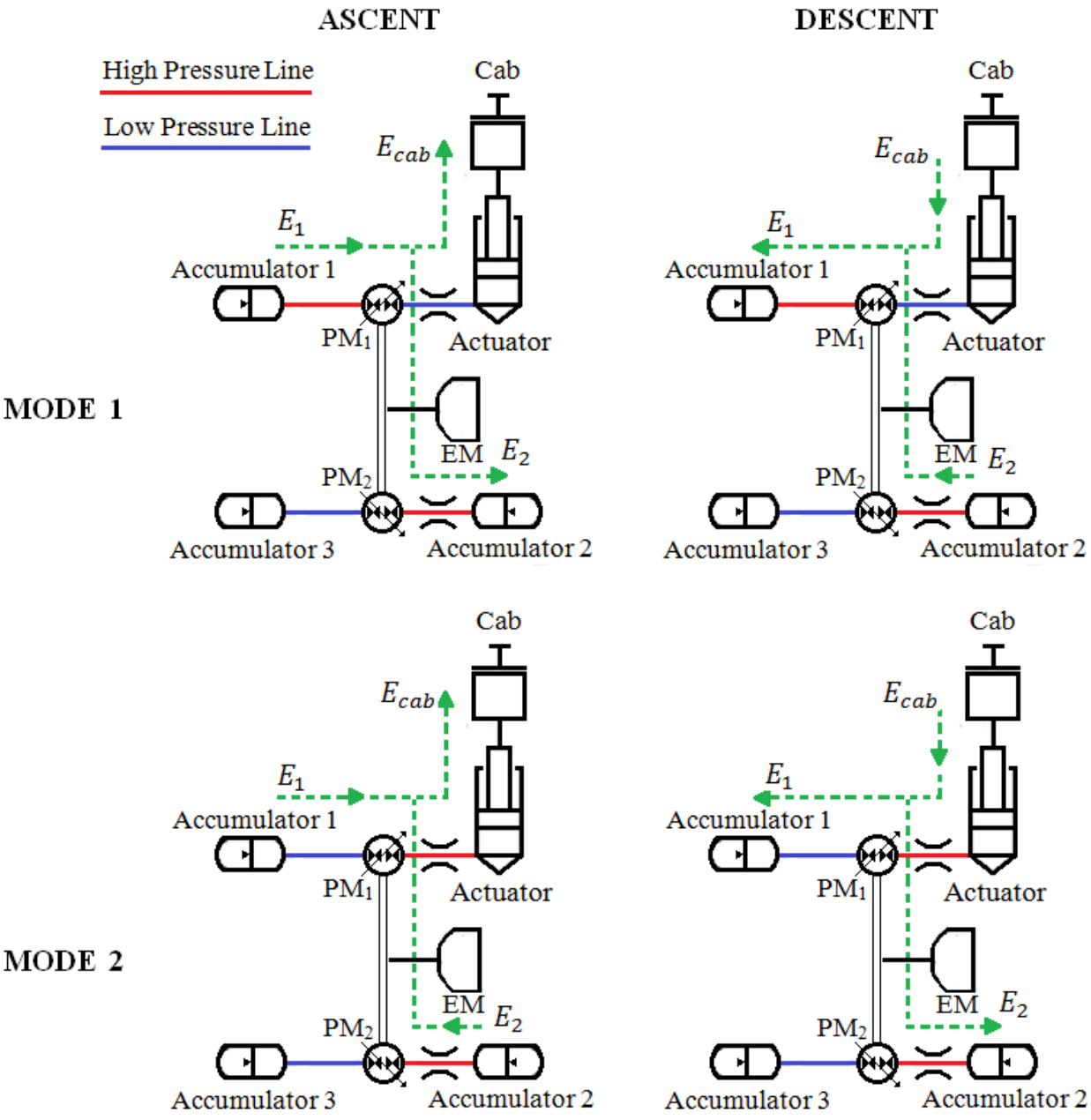

Figure B1: Energy flow through each operating mode during ascent and descent

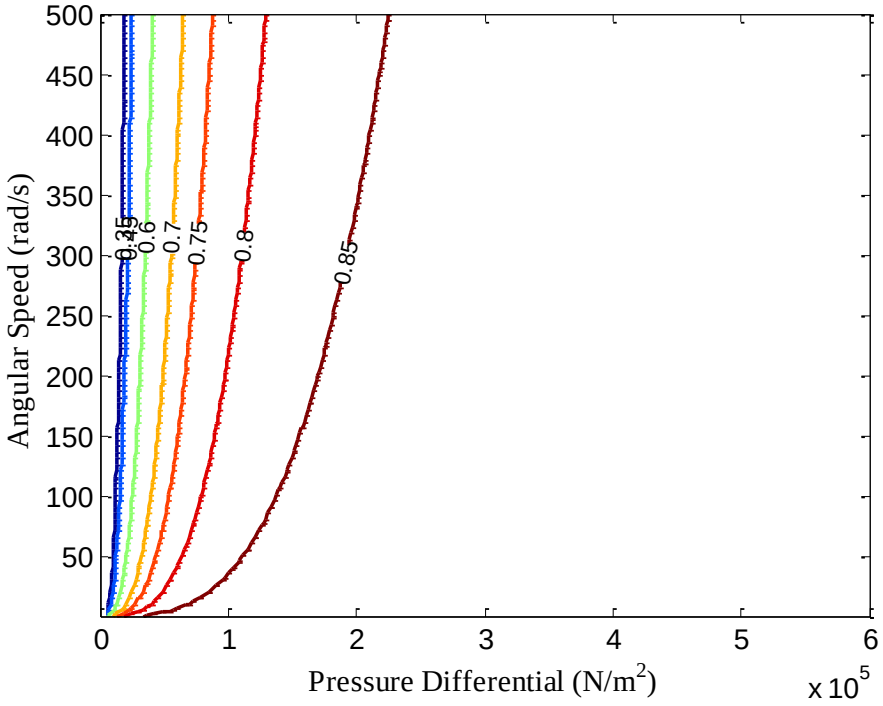

Figure B2: PM efficiency contours; constant displacement

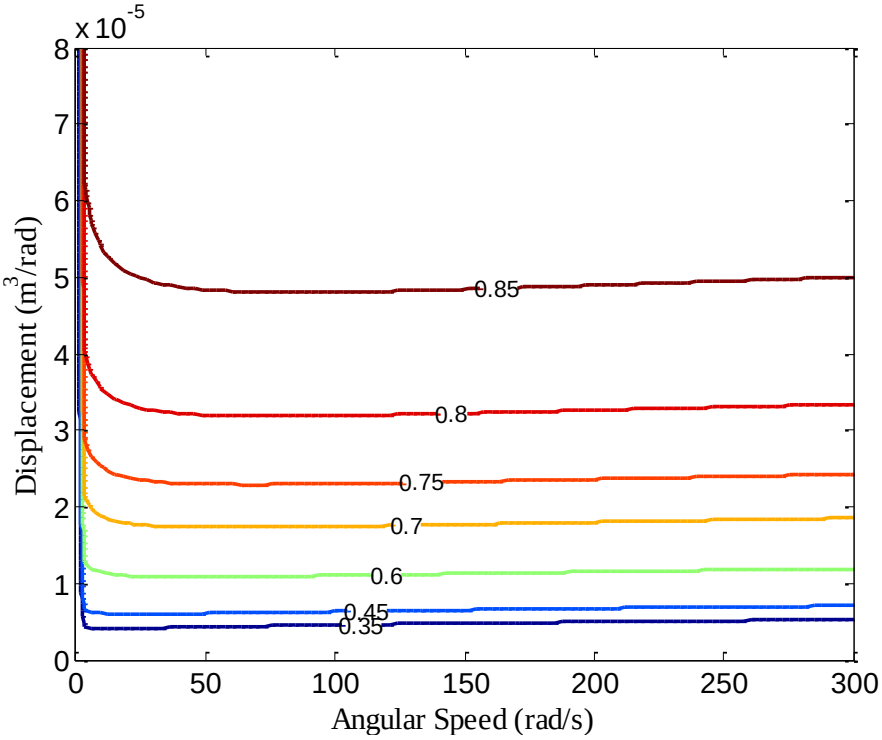

Figure B3: PM efficiency contours; constant differential pressure

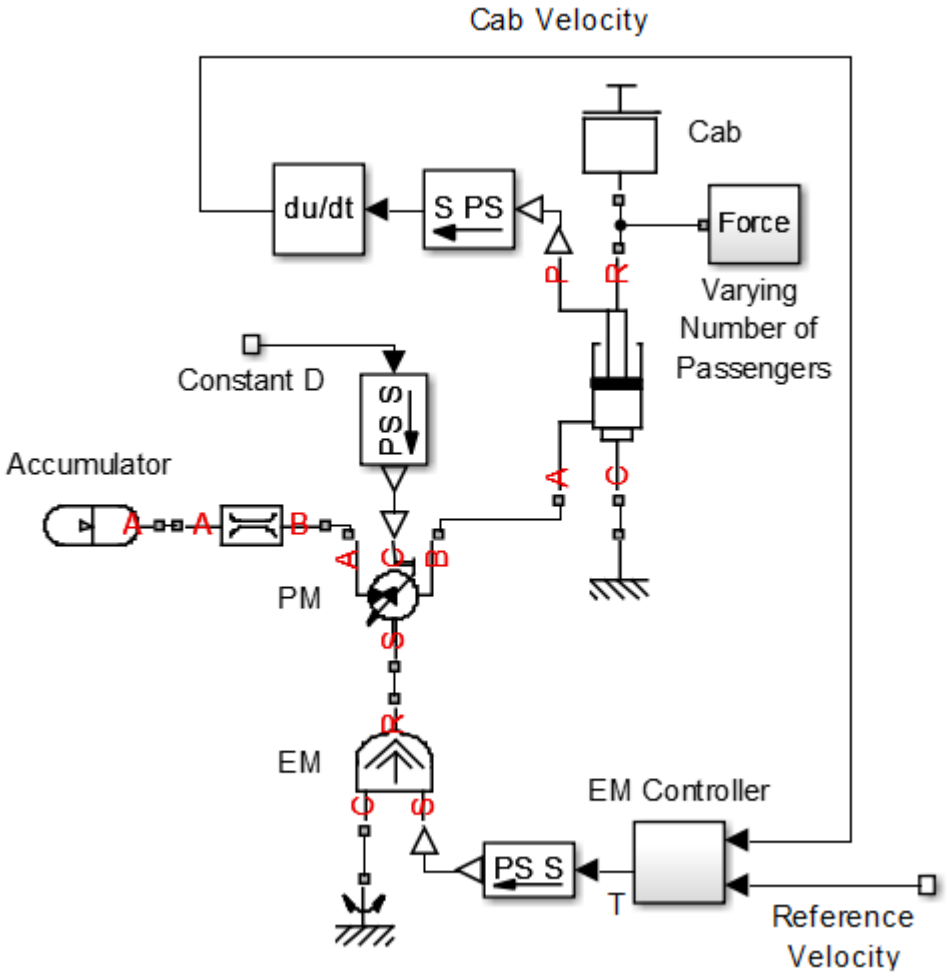

Figure B4: Simulink/SimScape model of the electrohydraulic system

Table B1: Parameters used for the SimScape model of the hydraulic architecture

Cab			
Mass (kg)	1100-2080		
Cylinder			
Area (m^2)	0.0036		
Stroke (m)	20		
	Accumulator 1	**Accumulator 2**	**Accumulator 3**
Capacity (m^3)	0.15	0.14	0.11
Preload Pressure (Pa)	9.25E+05	1.03E+07	6.90E+05
Initial Volume (m^3)	0.087	0.021	0
	PM_1	**PM_2**	
Displacement (m^3/rad)	4.23E-05	1.15E-05	
	Hydraulic Resistance 1	**Hydraulic Resistance 2**	
Area (m^2)	0.006	0.006	
Flow Discharge Coeff.	0.7	0.7	
	PM_1 Controller	**PM_2 Controller**	
P Gain (s-m^2/rad)	-4E-5	4E-5	
I Gain (m^2/rad)	-9E-5	9E-5	
	EM Controller		
P Gain (N-s)	-0.01		
I Gain (N)	0		
Reference Pressure (Pa)	1.32E7		
	Motion		
Distance per Floor (m)	3.65		
Max. Velocity (m/s)	0.63		
Max. Acceleration (m/s^2)	0.75		

Table B2: Parameters used for the SimScape model of the electrohydraulic system

	Cab
Mass (kg)	1100-2080
	Cylinder
Area (m^2)	0.0036
Stroke (m)	20
	Accumulator
Capacity (m^3)	0.15
Preload Pressure (Pa)	9.25E+05
Initial Volume (m^3)	0.087
	PM
Displacement (m^3/rad)	4.23E-05
	Hydraulic Resistance
Area (m^2)	0.006
Flow Discharge Coeff.	0.7
	EM Controller
P Gain (N-s)	500
I Gain (N)	100

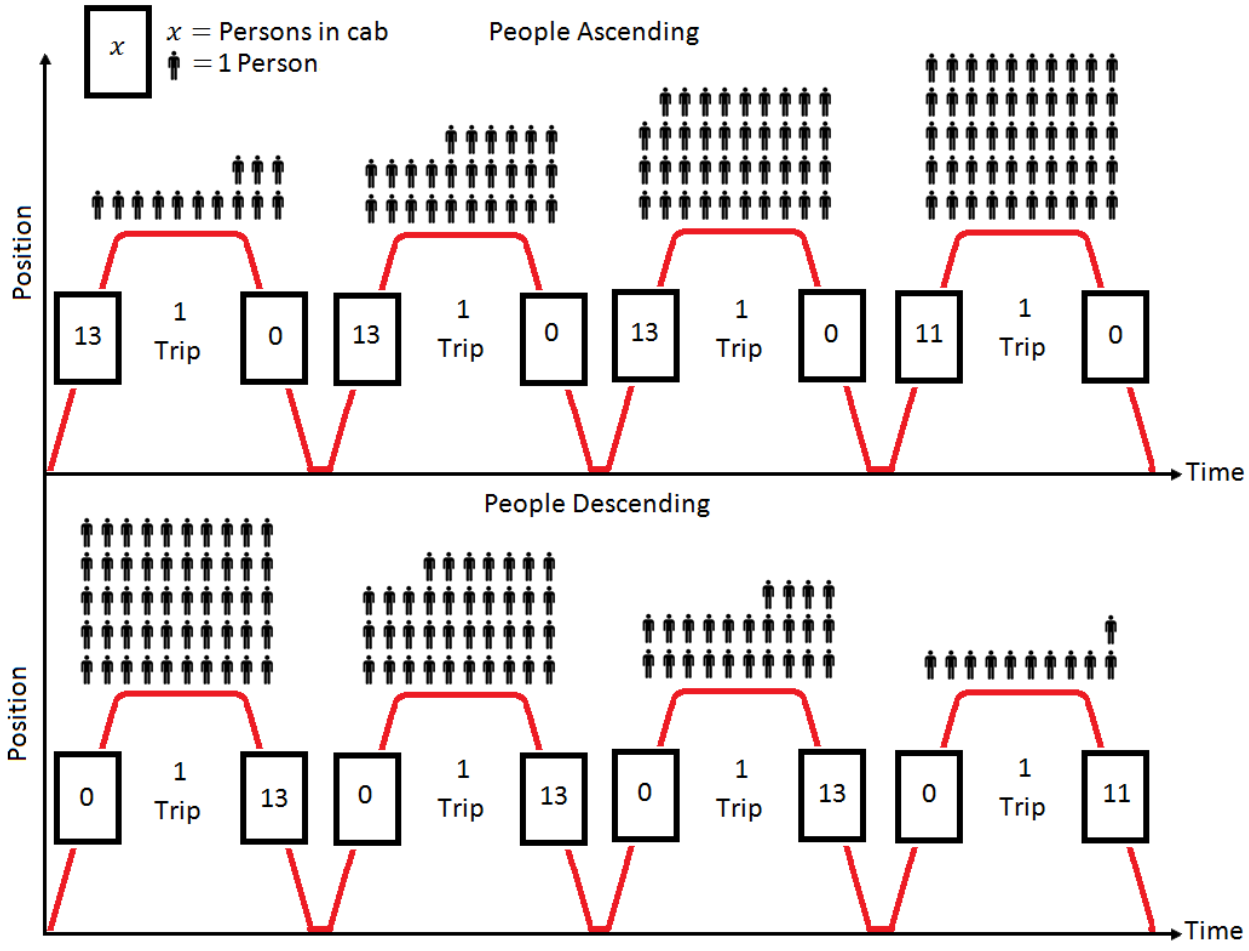

Figure B5: Full day operation for a cab load of 13 people for one floor; 8 trips per floor, for 3 floors (2nd, 3rd, and 4th) yields 24 trips total and 150 people moved

Table B3: Number of trips for a full day operation at each cab load

Cab Load (Persons)	1	2	3	4	5	6	7	8	9	10	11	12	13	14
Trips	300	150	102	78	60	54	48	42	36	30	30	30	24	24

APPENDIX C

SUPPLEMENTARY MATERIAL TO CHAPTER 3

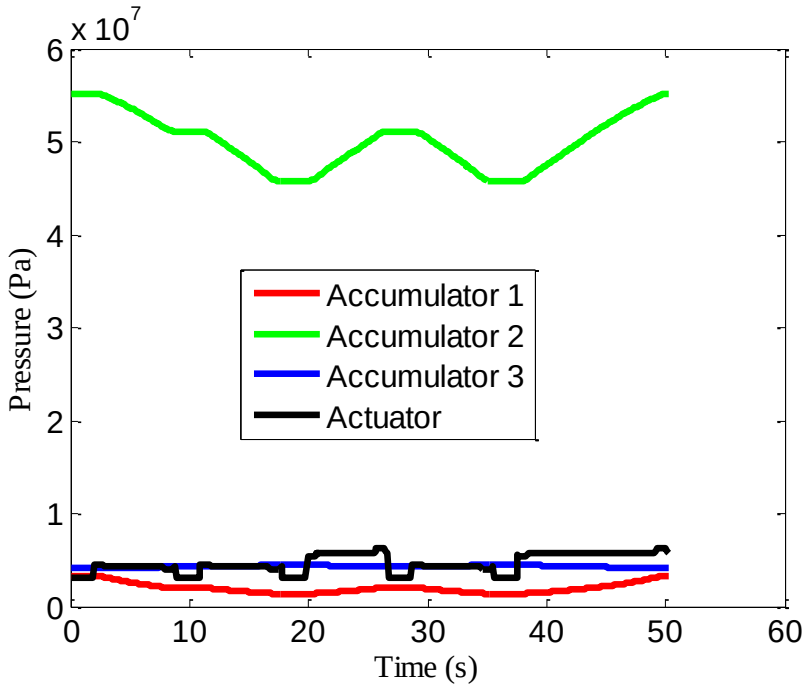

Figure C1: State path suggested by Dynamic Programming: Load Cycle 1

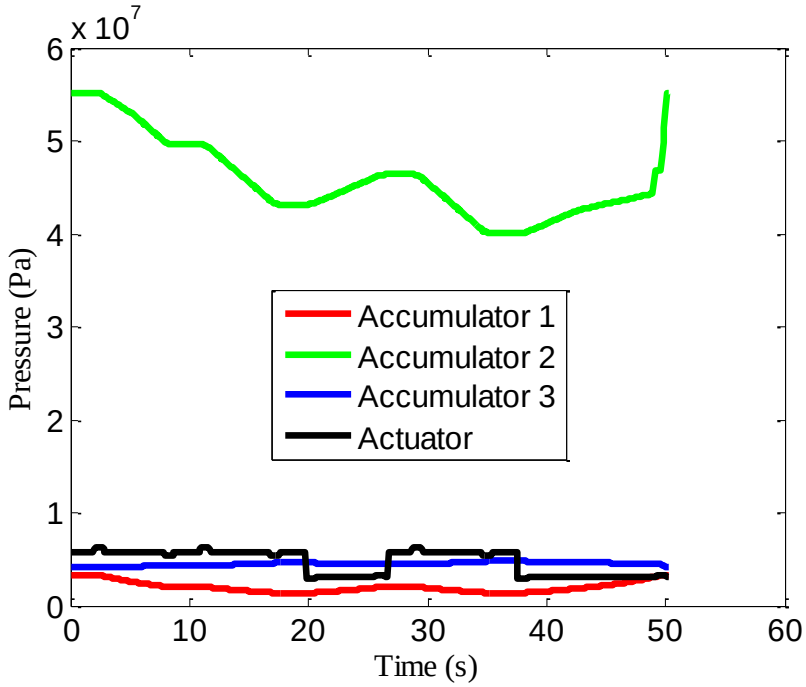

Figure C2: State path suggested by Dynamic Programming: Load Cycle 2

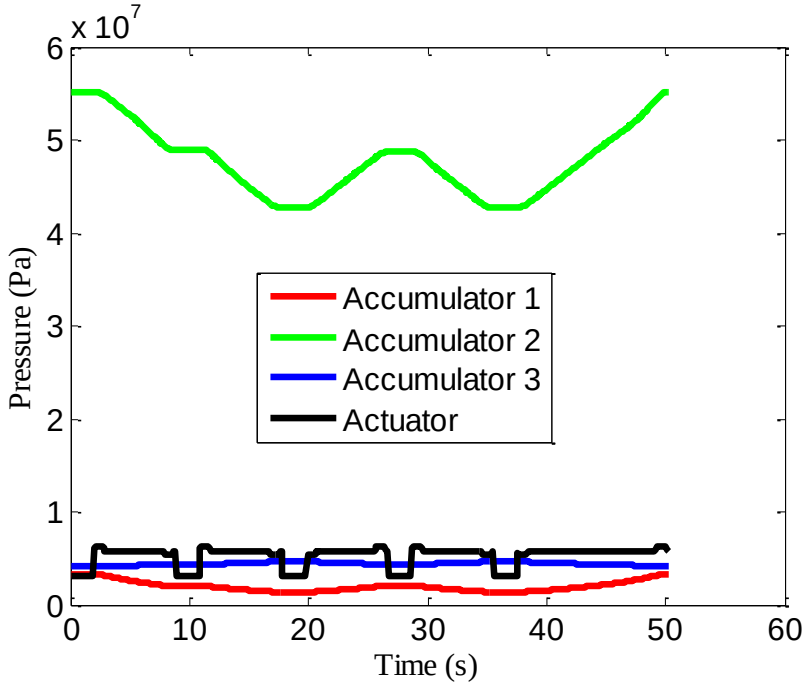

Figure C3: State path suggested by Dynamic Programming: Load Cycle 3

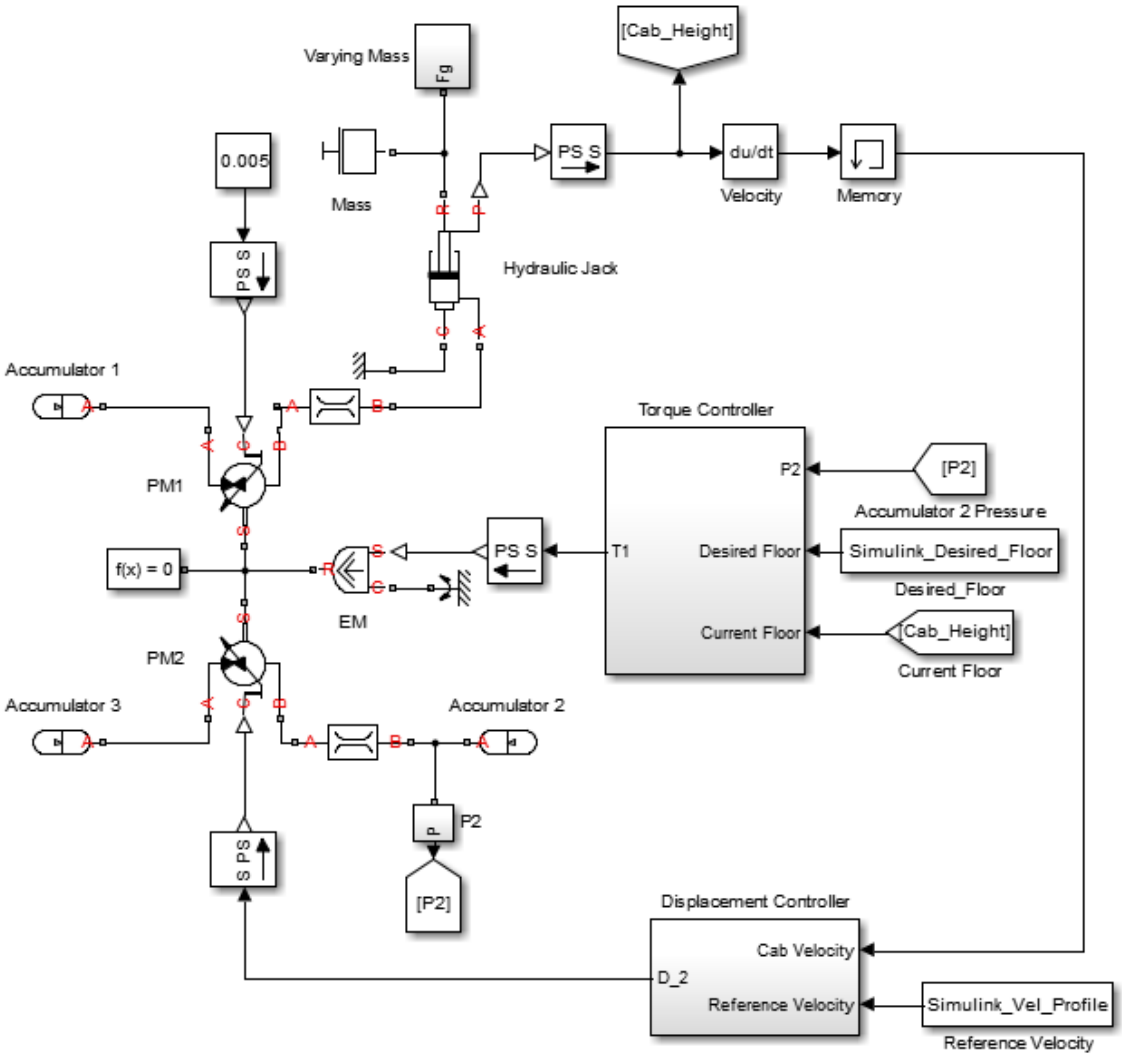

Figure C4: Simulink diagram of DP-informed ruled-based controlled architecture

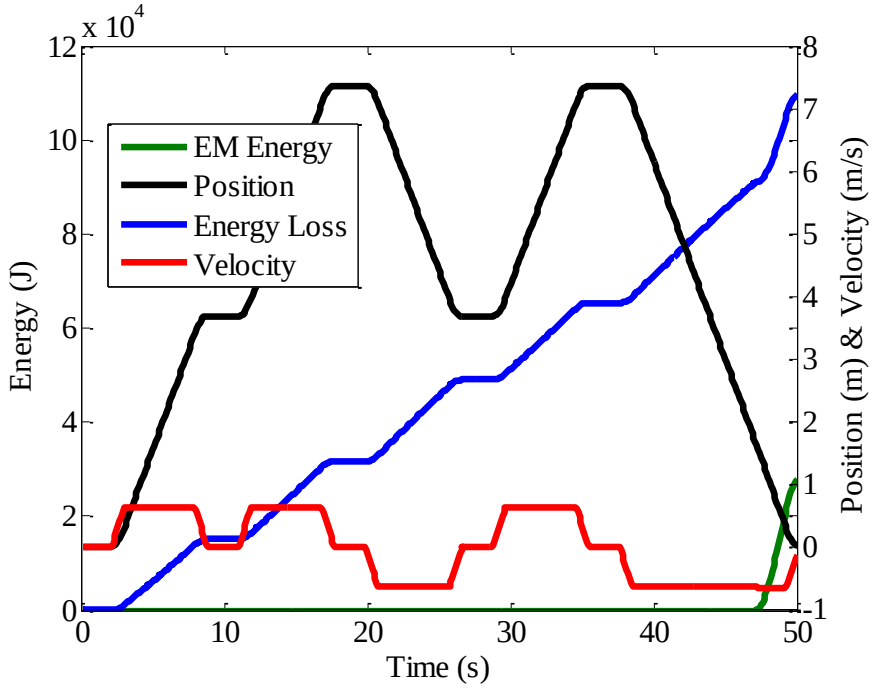

Figure C5: Architecture performance using DP-informed rule-based controller: Load Cycle 2.

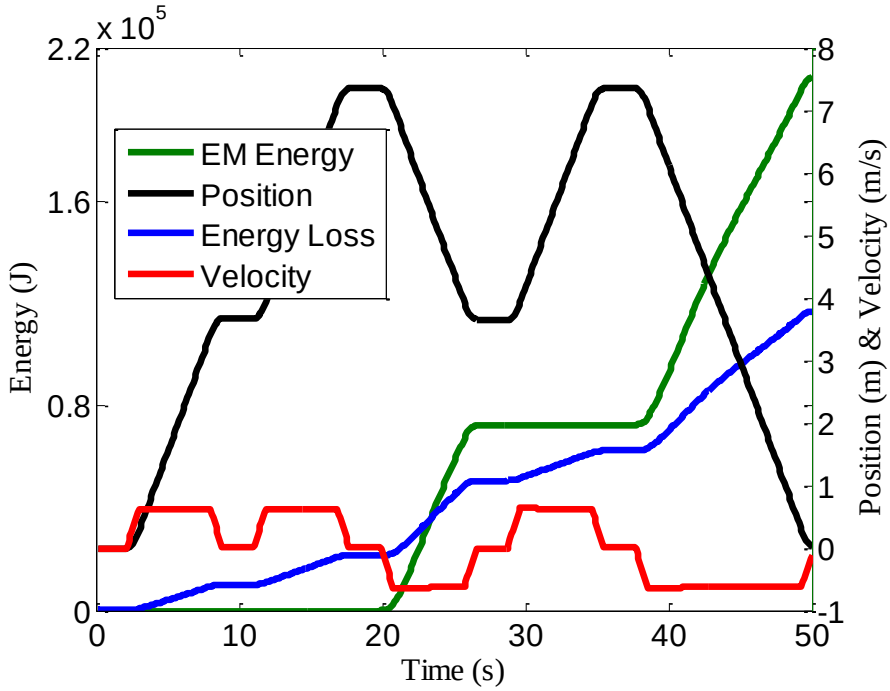

Figure C6: Architecture performance using DP-informed rule-based controller: Load Cycle 3.

REFERENCES

[1] Wang, M., and Li, P. Y., "Displacement Control of Hydraulic Actuators Using a Passivity Based Nonlinear Controller," Proc. ASME 2012 5th Annual Dynamic Systems and Control Conference joint with the JSME 2012 11th Motion and Vibration Conference, American Society of Mechanical Engineers, pp. 715-721.

[2] Xu, J., Zhang, B., and Lin, B., 2006, "Energy Consumption Characteristics of VVVF Controlled Hydraulic Elevators " Chinese Journal of Mechanical Engineering, 42(8), pp. 137-141.

[3] Zimmerman, J. D., Pelosi, M., Williamson, C. A., and Ivantysynova, M., "Energy consumption of an LS excavator hydraulic system," Proc. ASME International Mechanical Engineering Congress and Exposition, pp. 117-126.

[4] Grabbel, J., and Ivantysynova, M., 2005, "An investigation of swash plate control concepts for displacement controlled actuators," International Journal of Fluid Power, 6(2), pp. 19-36.

[5] Mitchell, J. P., 2001, "Load sensing hydraulic control system for variable displacement pump," Caterpillar Inc., United States of America.

[6] Oda, Y., and Shirai, K., 1997, "Displacement control system for variable displacement hydraulic pump," Kabushiki Kaisha Komatsu Seisakusho, United States of America.

[7] Zimmerman, J., 2008, "Design and Simulation of an Energy Saving Displacement-Controlled Actuation System for a Hydraulic Excavator," Master's Thesis, Purdue University, West Lafayette, IN.

[8] Celik, F., and Korbahti, B., 2008, "Why Hydraulic Elevators are So Popular? Part I.," Asansör Dünyasi, Blain Hydraulics

[9] Celik, F., and Korbahti, B., 2008, "Why Hydraulic Elevators are So Popular? Part II," Asansör Dünyasi, Blain Hydraulics.

[10] Xia, J., and Durfee, W. K., 2013, "Analysis of Small-Scale Hydraulic Actuation systems," Journal of Mechanical Design, 135(9), p. 091001.

[11] Manring, N. D., Mehta, V. S., Nelson, B. E., Graf, K. J., and Kuehn, J. L., 2013, "Increasing the Power Density for Axial-Piston Swash-Plate Type Hydrostatic Machines," Journal of Mechanical Design, 135(7), p. 071002.

[12] Verma, S., "Invention Story of Elevator," http://www.engineersgarage.com/invention-stories/elevator-history.

[13] Edwards, J. T., 1992, "Conserving energy in oil hydraulic elevator system," Elevator world, 40(7), pp. 51-52.

[14] Ran, L., 1998, "Study on a new type of speed control system and energy-saving in hydraulic elevator,"Ph. D. dissertation, Zhejiang University, Hangzhou, China.

[15] Shimoaki, M., 1992, "VVVF-controlled hydraulic elevators," Mitsubishi Electric Advance, 61, pp. 13-15.

[16] Xu, B., 2001, "Study on energy-saving control system of a VVVF hydraulic elevator using hydraulic accumulator,"Ph.D. dissertation, Zhejiang University, Hangzhou, China.

[17] Jianjie, L., Xu, B., and Yang, H., 2003, "Study on Energy Consumption Characteristics of VVVF Controlled Hydraulic Elevators with Pressure Accumulators," Chinese Journal of Mechanical Engineering, 39(7), pp. 63-67.

[18] Zürcher, J., and Moser, D., 2003, "Hydraulic elevator, comprising a pressure accumulator which acts as a counterweight and a method for controlling and regulating an elevator of this type," Bucher Hydraulics Ag, United States of America.

[19] Yang, H., Sun, W., and Xu, B., 2007, "New Investigation in Energy Regeneration of Hydraulic Elevators," IEEE/ASME Transaction on Mechatronics, 12(5), pp. 519-526.

[20] Moser, D., 2005, "Hydraulic elevator with an accumulator," Bucher Hydraulics Ag, United States of America.

[21] Minav, T. A., Laurilla, L. I. E., Immonen, P. A., Haapala, M. E., and Pyrhonen, J. J., 2009, "Electric Energy Recovery System Efficiency in a Hydraulic Forklift," EUROCON 2009, IEEE, St. Petersburg, pp. 758-765.

[22] Minav, T. A., Virtanen, A., Laurila, L., and Pyrhonen, J., 2012, "Storage of Energy Recovered from an Industrial Forklift," Automation in Construction, 22, pp. 506-515.

[23] Ven, J. V. d., 2009, "Increasing Hydraulic Energy Storage Capacity: Flywheel-Accumulator," International Journal of Fluid Power, 10(3), pp. 41-50.

[24] Hung, H. T., and Kwan, A. K., "A study on the position control of hydraulic cylinder driven by hydraulic transformer using disturbance observer," Proc. International Conference on Control, Automation and Systems, S. K. Kim, ed., IEEE, pp. 2634-2639.

[25] Chaturvedi, D. K., 2010, Modeling and Simulation of Systems Using MATLAB and Simulink, Taylor and Francis Group, LLC.

[26] Lumkes, J., Batdorff, M., and Mahrenholz, J., 2009, "Model Development and Experimental Analysis of a Virtually Variable Displacement Pump System," International Journal of Fluid Power, 10(3), pp. 17-27.

[27] Manring, N., 2003, "Valve-plate design for an axial piston pump operating at low displacements," Journal of Mechanical Design, 125(1), pp. 200-205.

[28] Wang, S., 2012, "Improving the Volumetric Efficiency of the Axial Piston Pump," Journal of Mechanical Design, 134(11), p. 111001.

[29] Hicks, T. G., and Edwards, T. W., 1971, Pump Application Engineering, McGraw-Hill, NY.

[30] Pei, D., 2012, "Development of Simulation Tools, Control Strategies, and a Hybrid Vehicle Prototype," Master's Thesis, Georgia Institute of Technology, Atlanta, GA.

[31] Pourmovahed, A., Baum, S. A., Fronczak, F. J., and Beachley, N. H., 1988, "Experimental Evaluation of Hydraulic Accumulator Efficiency With and Without Elastomeric Foam," Journal of Propulsion, 4(2), pp. 185-192.

[32] Larminie, J., and Lowry, J., 2012, Electric Vehicle Technology Explained, John Wiley & Sons Ltd.

[33] Donne, M. S., Tilley, D. G., and Richards, W., 1995, "The use of multi-objective parallel genetic algorithms to aid fluid power system design," Journal of Systems and Control Engineering, 209, pp. 53-61.

[34] Dubi, A., 2000, Monte Carlo Applications in Systems Engineering, John Wiley & Sons Ltd, West Sussex, England.

[35] Sundstrom, O., and Guzzella, L., 2009, "A Generic Dynamic Programming Matlab Function," IEEE International Conference on Control Applications, IEEE, Saint Petersburg, Russia.

[36] Bellman, R., 1957, Dynamic programming, Princeton University Press.

[37] Minav, T. A., Filatov, D., Pyrhonen, J., and Pietola, M., 2013, "Modelling of a working cycle of an electro-hydraulic forklift in Matlab Simulink," International Review on Modelling and Simulations, 6(6).